Lanthanide-based molecular alloys with hydroxyterephthalate: A versatile system

J. Wang, Yan Suffren, C. Daiguebonne, Kevin Bernot, Guillaume Calvez, Stéphane Freslon, O. Guillou

Lanthanide-based molecular alloys with hydroxy-terephthalate: A versatile system.

Jinzeng Wang, Yan Suffren, Carole Daiguebonne, Kevin Bernot, Guillaume Calvez, Stéphane Freslon and Olivier Guillou*.

Univ Rennes, INSA Rennes, CNRS UMR 6226 "Institut des Sciences Chimiques de Rennes", F-35708 Rennes, France.

* To whom correspondence should be addressed: Olivier.guillou@insa-rennes.fr

ABSTRACT

Reactions in water between a lanthanide chloride and the di-sodium salt of 2-hydroxy-terephthallic acid (H_2hbdc) lead to six families of lanthanide-based coordination polymers depending on the lanthanide ion and on the crystal growth method. Compounds that constitute family **F1** have general chemical formula $[Ln(Hhbdc)(hbdc)\cdot 9H_2O]_\infty$ with Ln = La-Nd and have been obtained by slow evaporation. $[Ln_2(hbdc)_3(H_2O)_6\cdot 4H_2O]_\infty$ with Ln = Sm-Eu constitute family **F2** and have been obtained by solvo-thermal synthesis. Family **F3** gathers compounds, obtained by solvo-thermal method, with general chemical formula $[Ln_2(hbdc)_3(H_2O)_4\cdot 4H_2O]_\infty$ with Ln = Ho-Lu plus Y and compounds obtained by slow diffusion through gels with Ln = Eu-Tb. $[Ln(Hhbdc)(hbdc)(H_2O)_3\cdot H_2O]_\infty$ with Ln = Tb-Dy have been obtained by solvo-thermal methods and constitute family **F4**. $[Gd_2(hbdc)_3(H_2O)_8\cdot 6H_2O]_\infty$ (**F5**) has been obtained by slow evaporation. The last family (**F6**) gathers compounds with general chemical formula $[Ln_2(hbdc)_3(H_2O)_8\cdot 2H_2O]_\infty$ with Ln = Nd-Tb that have been obtained by slow diffusion through gel media. Gd-based micro-crystalline powders can be obtained by direct mixing of aqueous solutions of Gd^{3+} and of $hbdc^{2-}$. Unexpectedly, the micro-crystalline powder belongs to **F5** when the lanthanide solution is added to the ligand one and to **F6** when it is the opposite. This phenomenon is also observed for Tb- and/or Eu-based hetero-lanthanide coordination polymers. Their optical properties have been studied in details.

INTRODUCTION

For almost two decades there is a growing interest for luminescent lanthanide-based coordination polymers because of their potential applications in various technological fields[1-4] such as chemical sensing[5-7], lighting and display[8-9], thermometry[10-11] and fight against counterfeiting[12], for examples. Because lanthanide ions can be considered as hard acids according to Pearson's theory,[13] the choice of the ligand is of first importance as far as structural organization is concerned. Lanthanide-based coordination polymers with terephthalate have been extensively studied because of their great structural diversity[14] and their high optical applicative potential.[15-16] Their hydroxy-derivatives are appealing because of potential influence of the hydroxyl group on the optical properties and/or on the crystal structure. Indeed, the donor hydroxyl function can induce photon-induced electron transfer (PET) mechanism[17] and can be involved in a H-bonds network. Therefore, we have undertaken a study of lanthanide-based coordination polymers with 2-hydroxy-terephthalate ($hbdc^{2-}$) ligand (scheme 1).

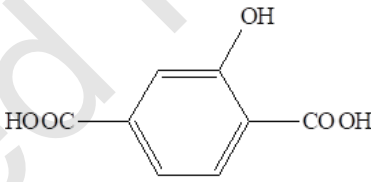

Scheme 1. Schematic representation of 2-hydroxy-terephthalic acid (H_2hdbc).

To the best of our knowledge, only one lanthanide-based coordination polymer with this ligand has been reported to date: $[Eu_2(hbdc)_3(H_2O]_\infty$.[18] This compound, obtained by solvo-thermal technics, presents a 3D crystal structure. It shows good efficiency in ratiometric Fe^{3+} ions sensing.

In this paper, six new families of lanthanide based coordination polymers with 2-hydroxy-terephthalate are described and their luminescent properties as well.

EXPERIMENTAL SECTION

2-hydroxy-terephthalic acid was purchased from TCI and used without further purification. Lanthanide oxides (4N) were purchased from Ampère. Lanthanide chlorides were prepared according to established procedures.[19] Tetramethylorthosilicate was purchased from Acros Organics. Gels were prepared according to previously described procedures.[20-22]

Synthesis of the single-crystals of the coordination polymers

Three different synthetic methods have been used to grow single-crystals: solvo-thermal, slow evaporation and diffusion through gel methods. Results of the crystal growth experiments are summarized in Table 1.

Table 1. Summary of the successful crystal growths.

Structural family	La	Ce	Pr	Nd	Sm	Eu	Gd	Tb	Dy	Y	Ho	Er	Tm	Yb	Lu
F1	Slow evaporation														
F2															
F3										Solvo-thermal synthesis					
F4															
F5															
F6				Diffusion through gel											

Membership of a structural family or another has been assumed on the basis of powder X-ray diffraction diagrams recorded on microcrystalline powders made of crushed single crystals (Figures S2 to S5) or on the basis of cell parameters when single crystal were grown in gel medium.

Preparation of the lanthanide coordination polymers microcrystalline powders

A solution of a lanthanide chloride (Ln = La-Lu plus Y except Pm) (0.2 mmol in 5 mL of water) was added to an aqueous solution of $Na_2hbdc{\cdot}H_2O$ (0.3 mmol in 5 mL of water). The mixture was maintained under stirring during 48 hours for insuring better crystallinity.

The obtained white precipitate was filtered and dried under ambient conditions (the yield was about 90%). The microcrystalline powders have been classified into four structural families on the basis of their powder X-ray diffraction diagrams (Table 2 and Figure S6).

Table 2. Membership of a structural family of the homo-lanthanide coordination polymers microcrystalline powders.

	La Ce Pr Nd	Sm Eu	Gd	Tb Dy Y Ho Er Tm Yb Lu
Structural family	**F1**	**F2**	**F5**	Unknown phase
			F6	

It is noticeable that depending on the reactant that is added to the other, Gd-derivative crystallizes with structural type **F5** or **F6** (Figure S7).

In order to target brightness and color tuning, some hetero-lanthanide coordination polymers have also been prepared simply replacing, in the above described synthesis, the lanthanide solution by a solution that contains an appropriate mixture of lanthanide chlorides. Membership of one or another structural family was assumed on the basis of the powder X-ray diffraction diagrams of the microcrystalline powders (Figures S8 to S11 and Table 3). Their relative metallic contents were measured by EDS and are listed in Table S1. Identically to the Gd-based coordination polymers, the structural type adopted by Gd/Tb, Gd/Eu and Tb/Eu-based hetero-lanthanide coordination polymers depends on the reactants addition order: when the lanthanides solution is added to the ligand solution the structural type is **F5**; on the opposite, **F6** is obtained when the ligand solution is added to the lanthanides solution.

Table 3. Stuctural families of powders of the hetero-lanthanide coordination polymers versus *x*.

	x = 0	0.1	0.2	0.3	0.4	0.5	0.6	0.7	0.8	0.9	1
$Tb_{2x}Eu_{2-2x}$*	**F2**	**F5**									
$Tb_{2x}Eu_{2-2x}$†	**F2**	**F6**									
$Gd_{2x}Tb_{2-2x}$†		**F6**									
$Gd_{2x}Eu_{2-2x}$†	**F2**	**F6**									

* lanthanides solution is added to ligand solution
† ligand solution is added to lanthanides solution
Unknown phase in grey

Syntheses of the di-sodium salt of 2-hydroxy-terephthalic acid and of the single-crystals of the coordination polymers are available in Supporting Information section. Powder X-ray diffraction, thermal analysis, electron dispersive spectroscopy and optical measurements have been performed according to procedures that have been previously reported.[23] They are available in Supporting Information section.

Single-crystal X-ray diffraction.

Selected crystal and final structure refinement data are gathered in Table 4. Some other details are available in Supporting Information section.

Table 4. Selected crystal and final structure refinement data.						
	F1	**F2**	**F3**	**F4**	**F5**	**F6**
Molecular formula	$PrC_{16}H_{19}O_{15}$	$Sm_2C_{24}H_{32}O_{25}$	$Y_2C_{24}H_{28}O_{23}$	$TbC_{16}H_{17}O_{14}$	$Gd_4C_{48}H_{80}O_{58}$	$Gd_2C_{24}H_{32}O_{25}$
Formula weight ($g.mol^{-1}$)	592.22	1021.19	862.28	592.21	2214.12	1034.99
System	Cubic	Triclinic	Triclinic	Triclinic	Monoclinic	Monoclinic
Space group (n°)	$Ia\bar{3}$(206)	$P\bar{1}$(2)	$P\bar{1}$(2)	$P\bar{1}$(2)	$C2/c$(15)	$P2_1/c$(14)
a (Å)	26.9120(7)	7.9806(8)	9.3864(7)	9.4609(8)	16.982(2)	10.9491(14)
b (Å)	26.9120(7)	9.9540(9)	10.0102(7)	10.3877(9)	10.8156(15)	12.8463(16)
c (Å)	26.9120(7)	10.8426(11)	10.3408(8)	11.0504(8)	20.008 (2)	11.5619(14)
α (°)	90	74.620 (3)	107.622(3)	115.254(3)	90	90
β (°)	90	74.092(3)	99.379(3)	107.794 (3)	105.231(4)	102.493(4)
γ (°)	90	73.803 (3)	110.080 (3)	90.967(3)	90	90
V ($Å^3$)	19491.2(4)	778.67(13)	830.17(11)	921.44(13)	3545.8(7)	1587.7(3)
Z	24	1	1	2	2	2
D_{calc} ($g.cm^{-3}$)	1.211	2.178	1.725	2.134	2.074	2.165
R (%)	0.0907	0.0202	0.0280	0.0210	0.0272	0.0244
R_w (%)	0.2862	0.0522	0.0756	0.0531	0.0688	0.0632
GoF	1.353	1.153	1.053	1.068	1.061	1.078
CCDC entry	1913183	1913130	1913137	1913124	1913145	1913142

RESULTS AND DISCUSSION

Family F1. $[Ln(Hhbdc)(hbdc)\cdot 9H_2O]_\infty$ with Ln = La-Nd

Compounds that constitute this family (**F1**) have general chemical formula $[Ln(Hhbdc)(hbdc)\cdot 9H_2O]_\infty$ with Ln = La-Nd. They have been obtained as microcrystalline powders by direct precipitation and as single-crystals by slow evaporation of the filtrates. Crystal structure has been solved on the basis of the Pr-derivative. Iso-structurality of the other compounds has been assumed on the basis of their powder X-ray diffraction diagrams (Figure S2). $[Pr(Hhbdc)(hbdc)\cdot 9H_2O]_\infty$ crystalizes in the cubic system, space group $Ia\bar{3}$ (n°206). It is noticeable that these compounds are isomorphous to $[Ln(abdc)(Habdc)\cdot nH_2O]_\infty$ with Ln = La-Eu, $8 \leq n \leq 11$ where H_2abdc stands for 2-amino-terephthalic acid, that have been previously described.[24-25] In this crystal structure half of the ligands are once deprotonated as confirmed by the IR spectroscopy (Figure S12). Therefore, there are two types of ligand, $Hhbdc^-$ and $hbdc^{2-}$, in the chemical formula of the compound. There are two Pr^{3+} ions in the asymmetric unit. $Pr1^{3+}$ is twelve coordinated by six chelating carboxylate groups from six different ligands to form an icosahedron (Figure 1). $Pr2^{3+}$ is coordinated by nine oxygen atoms: three out of them from three different monodentate ligands and the six other from three different bidentate ligands. The coordination polyhedron can be described as a distorted tricapped trigonal prism (Figure 1).

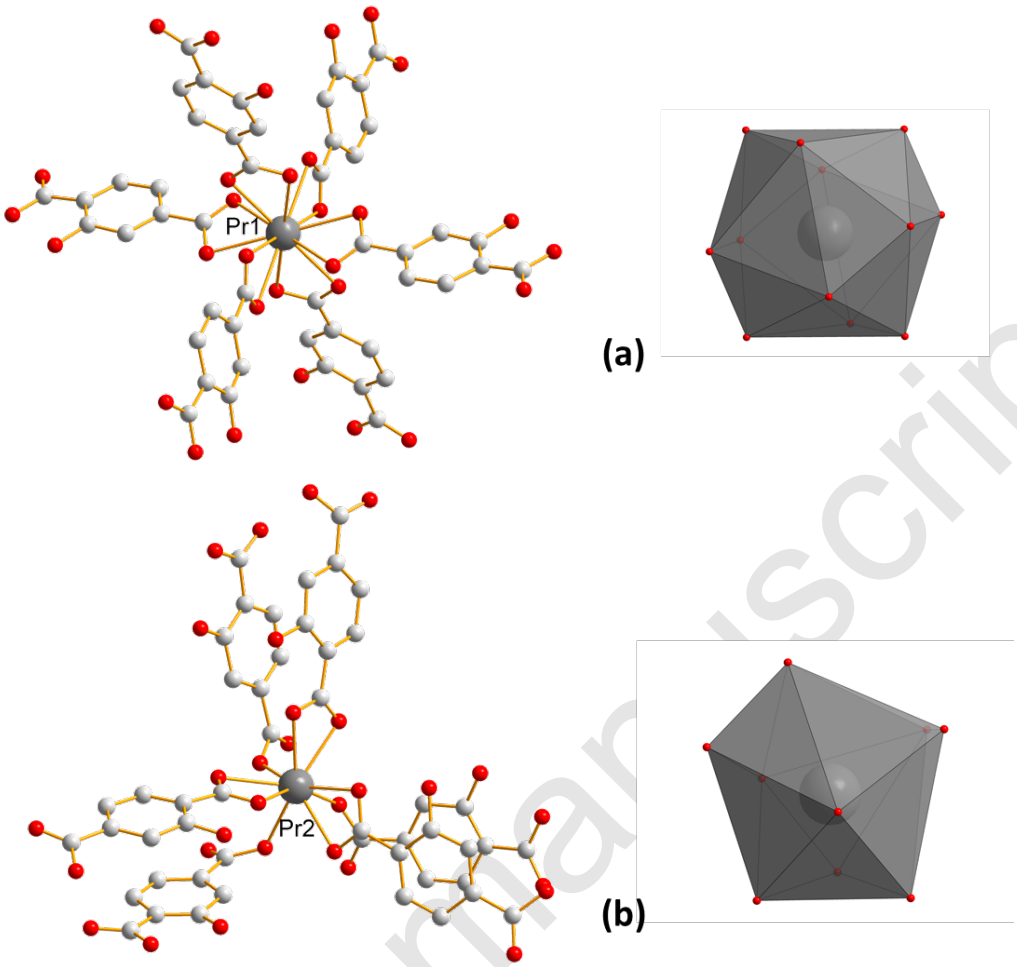

Figure 1. Coordination environments and coordination polyhedrons of $Pr1^{3+}$ (a), $Pr2^{3+}$ (b) in $[Pr(Hhbdc)(hbdc)\cdot 9H_2O]_\infty$ (**F1**).

Each $Pr1^{3+}$ is bound to two $Pr2^{3+}$ through carboxylate groups, to form a tri-nuclear unit (Figure 2) which prevents the entrance of coordinated water molecules in the coordination spheres. The shortest distance between $Pr1^{3+}$ and $Pr2^{3+}$ inside a tri-nuclear unit is 3.9407(5) Å. The Pr-Pr distance between Pr^{3+} ions that belong to adjacent tri-nuclear units is 11.6346(5) Å. All ligands adopt the same coordination mode (Figure 2).

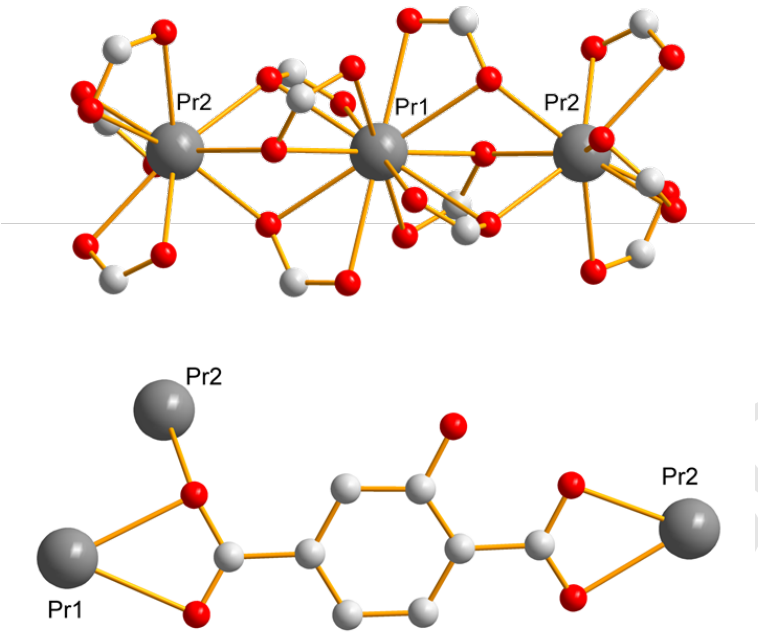

Figure 2. Schematic representation of the tri-nuclear unit that consists of $Pr1^{3+}$ and $Pr2^{3+}$ (parts of the ligand are omitted for clarity) (top). Coordination mode of the ligand (bottom) in $[Pr(Hhbdc)(hbdc)\cdot 9H_2O]_\infty$ (**F1**).

Each tri-nuclear unit is linked to twelve ligands which can be seen as six bridges if pairs of ligands are regarded as connections. This connection mode generates the cubic molecular skeleton (Figure 3). This crystal structure presents large square-section (11 x 11 $Å^2$) channels in which crystallization water molecules are localized. These crystallization water molecules were not precisely localized by single X-ray diffraction (which explains the bad GoF value). However, the overall number of crystallization water molecules was confirmed by thermo-gravimetric analysis (Figure S13).

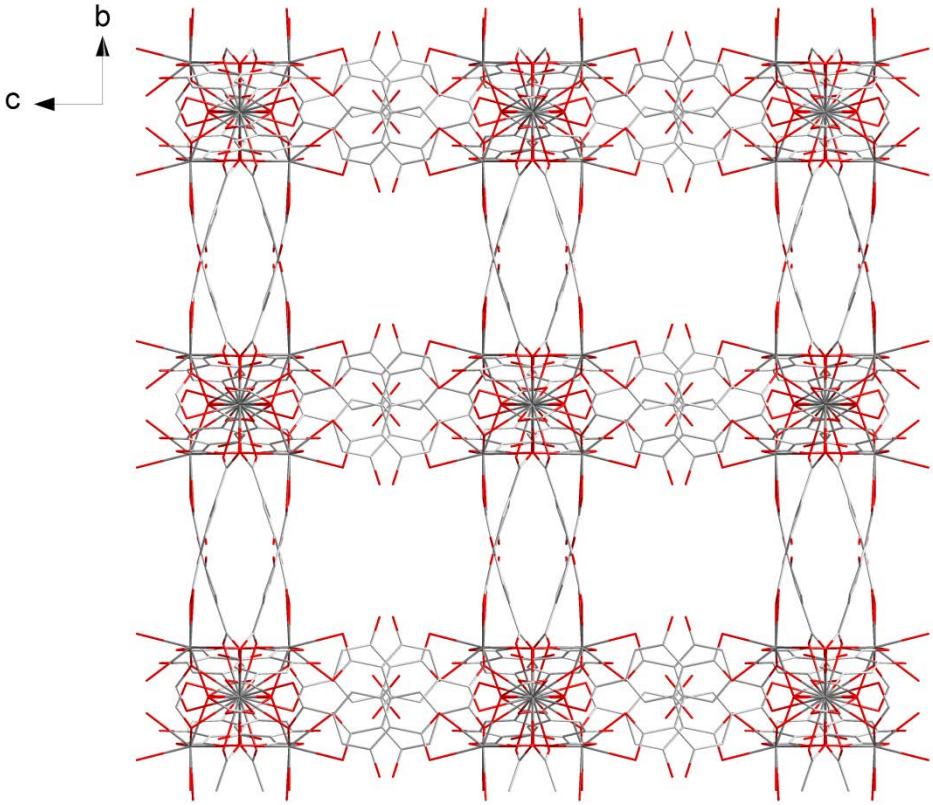

Figure 3. Projection view along the *a*-axis of $[Pr(Hhbdc)(hbdc)\cdot 9H_2O]_\infty$ (**F1**). Crystallization water molecules are omitted for clarity.

Solid-state excitation and emission spectra of $[Ln(Hhbdc)(hbdc)\cdot 9H_2O]_\infty$ (Ln = La-Nd) have been recorded at room temperature. The Pr^{3+}-derivative shows a weak emission in the visible and in the near infrared domains (Figure 4 top). The Nd^{3+}-derivative presents luminescent properties in the NIR region (Figure 4 bottom) under direct f-f excitation of the Nd^{3+} ion (λ_{exc} = 584 nm and λ_{exc} = 803 nm) as well as by antenna effect[26] (λ_{exc} = 326 nm).

Emission intensity under excitation at 326 nm is only a little bit stronger than that observed under excitations at 584 nm and 803 nm, which indicates a weakly efficient antenna effect.

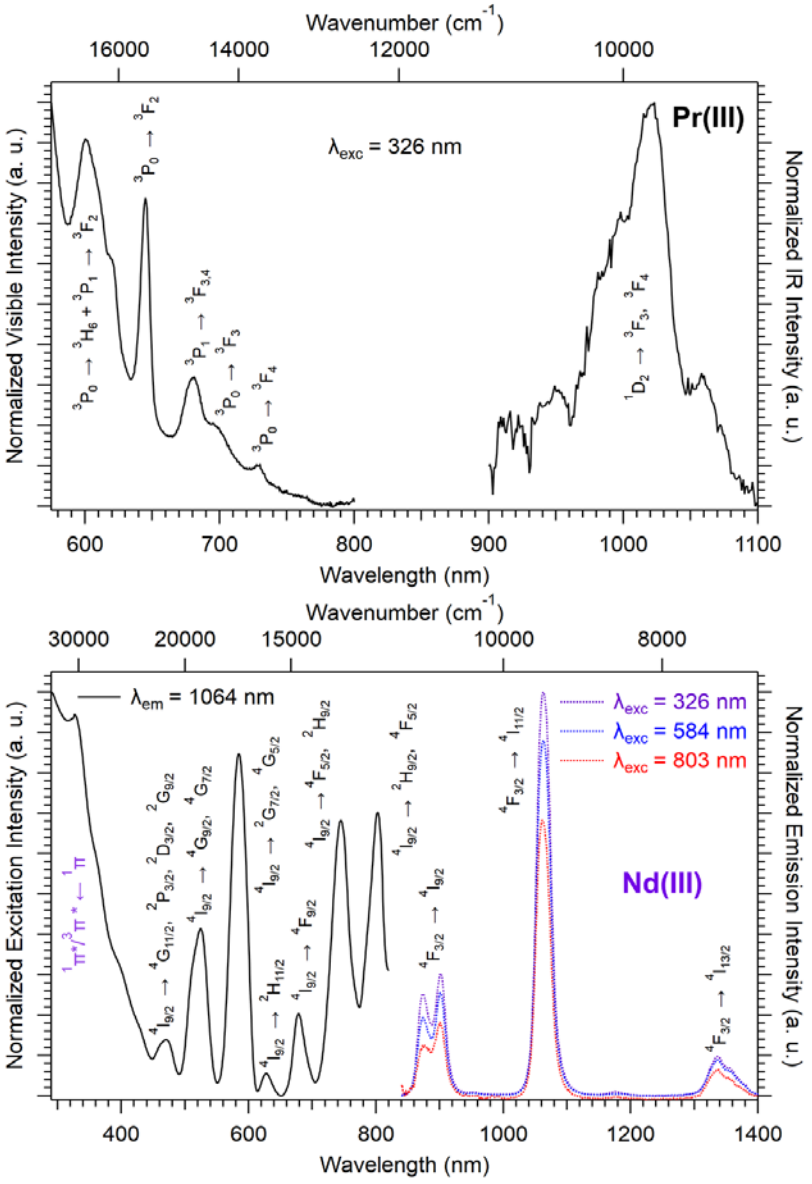

Figure 4. Solid-state visible and infrared emission spectra of [Pr(Hhbdc)(hbdc)·9H_2O]$_\infty$ (**F1**) at room temperature (top). Solid-state excitation and infrared emission spectra of [Nd(Hhbdc)(hbdc)·9H_2O]$_\infty$ (**F1**) at room temperature (bottom).

Family F2. [$Sm_2(hbdc)_3(H_2O)_6$·4H_2O]$_\infty$

Microcrystalline powders of Sm^{3+}- and Eu^{3+}-derivatives are iso-structural to [$Sm_2(hbdc)_3(H_2O)_6$·4H_2O]$_\infty$ (**F2**). Single-crystals have been obtained both by solvothermal method and diffusion in gel media with Sm^{3+}. [$Sm_2(hbdc)_3(H_2O)_6$·4H_2O]$_\infty$ crystallizes in the triclinic system, space group $P\bar{1}$. It is two-dimensional. Each Sm^{3+} ion is coordinated by six oxygen atoms from four different $hbdc^{2-}$ ligands and three oxygen atoms from three

coordination water molecules. The coordination polyhedron of the Sm^{3+} ion can be described as a spherical tricapped trigonal prism (Figure 5). The ligand $hbdc^{2-}$ presents two different coordination modes (Figure 5).

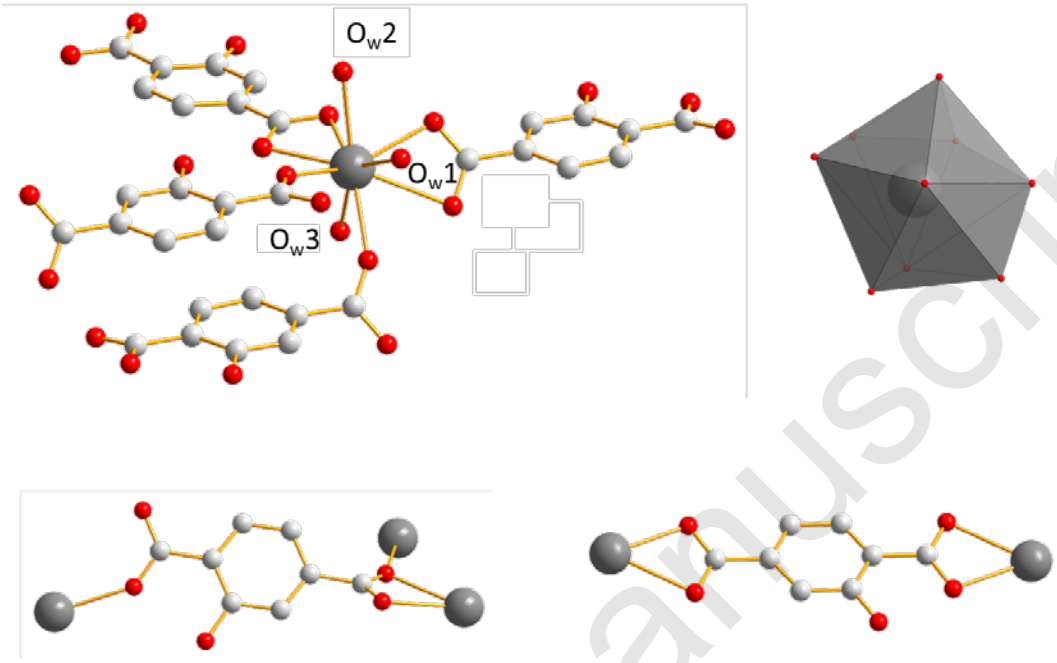

Figure 5. Coordination environment and coordination polyhedron of Sm^{3+} (top) and the two different coordination modes of the $hbdc^{2-}$ ligands (bottom) in $[Sm_2(hbdc)_3(H_2O)_6{\cdot}4H_2O]_\infty$ (**F2**).

The closest Sm^{3+} ions are bridged by the tridentate carboxylate group of the first coordination mode and form Sm^{3+}-based binuclear units. Inter-metallic distance inside a binuclear unit is 4.357(1) Å. Binuclear units are connected to each other by ligands in the second coordination mode through bidentate carboxylate groups, forming so a 1D molecular chain. Molecular chains are linked to each other through the second carboxylate group of the ligands that adopts the first coordination mode to generate 2D molecular layers. Intermetallic distances between Sm^{3+} ions that belong to different binuclear units inside a molecular layer are about 11.5 Å. Between two adjacent layers, the shortest Sm-Sm inter-metallic distances is 10.843(1) Å (Figure 6).

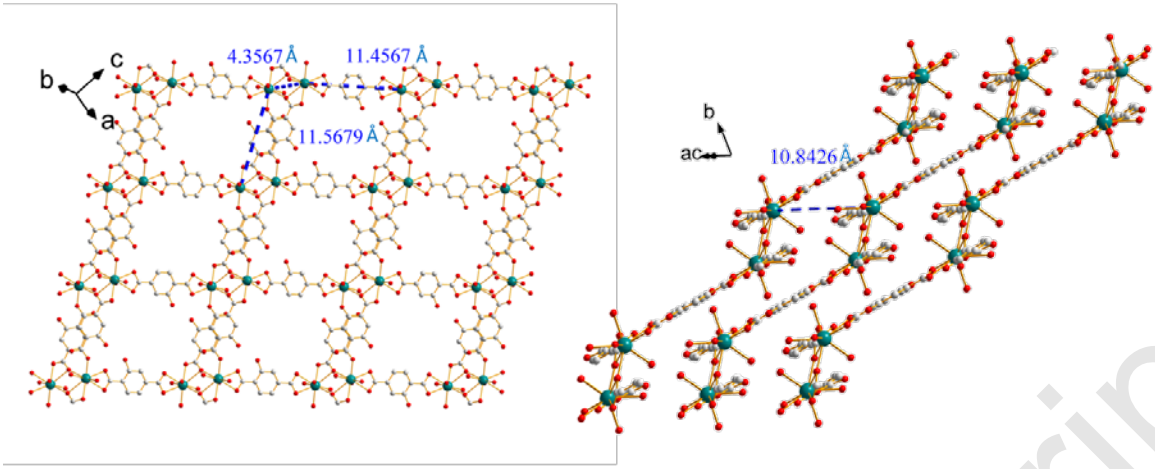

Figure 6. Projection views of a 2D molecular layer (left) and of the stacking of the molecular layers (right) of $[Sm_2(hbdc)_3(H_2O)_6{\cdot}4H_2O]_\infty$ (**F2**). Characteristic inter-metallic distances are indicated.

Crystallization water molecules are located in the channels that spread along the *b*-axis. These crystallization water molecules are strongly bounded to the molecular framework via an hydrogen bonds network that involve crystallization water molecules, oxygen atoms of the carboxylic groups and hydroxyl groups of the ligand (Figure 7). They are removed in two steps: between 120°C and 170°C (Figure S14)

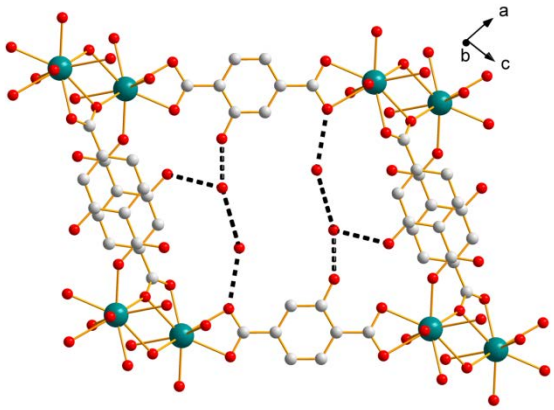

Figure 7. Hydrogen-bonds network (black broken lines) in $[Sm_2(hbdc)_3(H_2O)_6{\cdot}4H_2O]_\infty$ (**F2**).

Room temperature solid-state excitation and emission spectra and luminescence decay curves of $[Ln_2(hbdc)_3(H_2O)_6{\cdot}4H_2O]_\infty$ **(F2)** with Ln = Sm and Eu have been recorded (Figures 8 and S15).

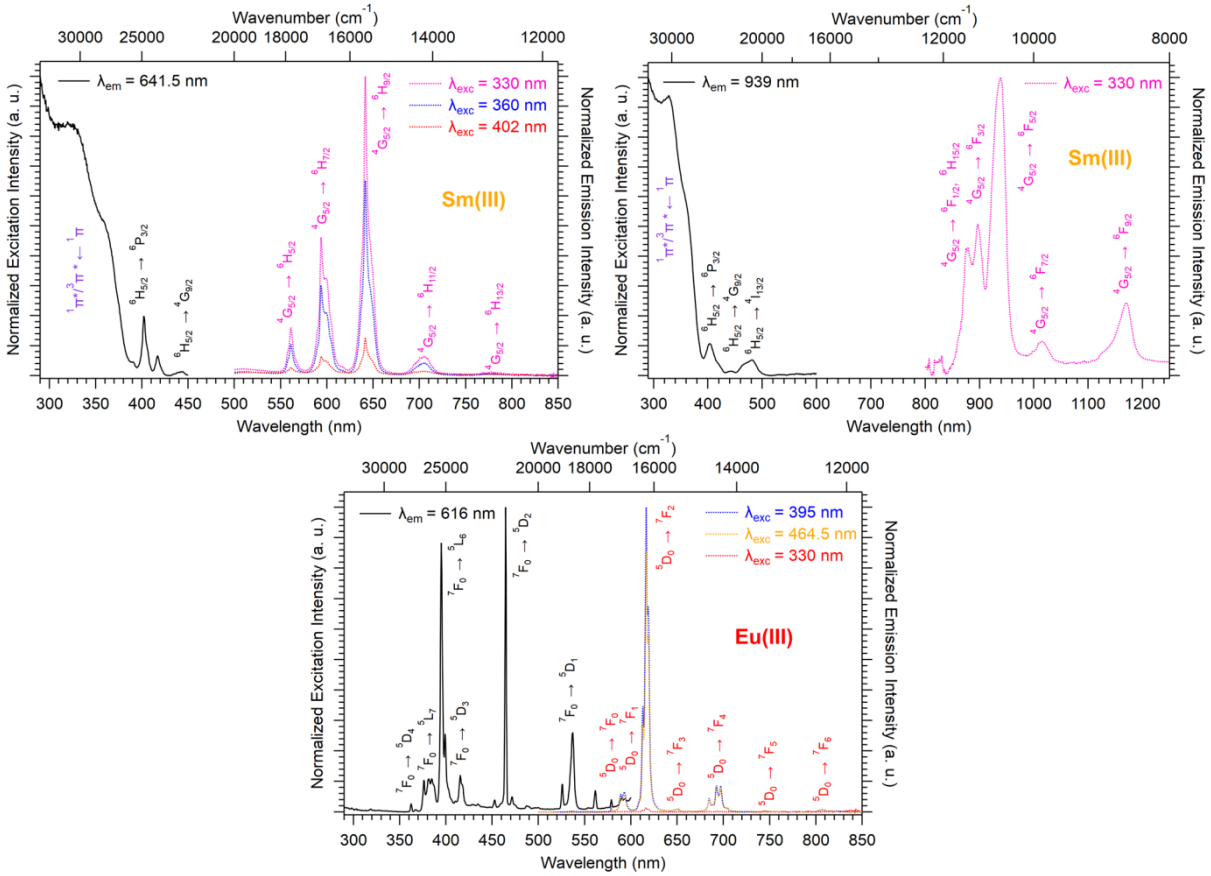

Figure 8. Room temperature solid-state excitation and emission spectra of $[Sm_2(hbdc)_3(H_2O)_6{\cdot}4H_2O]_\infty$ **(F2)** in the visible (top left) and IR (top right) regions, and of $[Eu_2(hbdc)_3(H_2O)_6{\cdot}4H_2O]_\infty$ **(F2)** (bottom). τ_{Eu} = 0.24(1) ms and Φ^{Eu}_{Eu} = 5.6(1)% with λ_{ex} = 395 nm. τ_{Sm} = 0.27(1) µs with λ_{ex} = 320 nm and Φ^{Lig}_{Sm} = 0.18(1)% with λ_{ex} = 330 nm.

Sm-derivative exhibits a strong luminescence under 330 nm excitation wavelength that corresponds to the $^1\pi^*/^3\pi^* \leftarrow {}^1\pi$ absorption band of the ligand. On the contrary, excitation spectrum of $[Eu_2(hbdc)_3(H_2O)_6{\cdot}4H_2O]_\infty$ **(F2)** (λ_{em} = 616 nm) presents no excitation band at this wavelength. This can be related to a photo-induced electron transfer (PET) mechanism that is commonly observed when an easily reducible lanthanide ion (such as Eu^{3+}) is in the vicinity of a donor group (such as –OH group) (Scheme 2).[7, 17, 27]

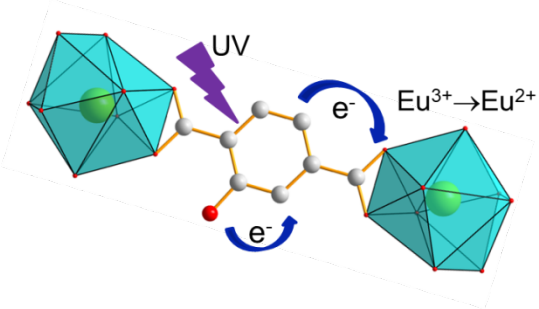

Scheme 2. Schematic representation of the PET mechanism for $[Eu_2(hbdc)_3(H_2O)_6{\cdot}4H_2O]_\infty$ (**F2**).

Family 3. $[Y_2(hbdc)_3(H_2O)_4{\cdot}4H_2O]_\infty$

Single-crystals of Ho^{3+}- to Lu^{3+}- and Y^{3+}-derivatives have been obtained by solvothermal method while those of Eu- to Tb-derivatives have been grown by slow diffusion through gel medium. All of them are isostructural. Their general chemical formula is $[Ln_2(hbdc)_3(H_2O)_4{\cdot}4H_2O]_\infty$ with Ln = Eu-Tb and Ho-Lu plus Y (**F3**). Hereafter, the crystal structure is described on the basis of the Y^{3+}-derivative. $[Y_2(hbdc)_3(H_2O)_4{\cdot}4H_2O]_\infty$ (**F3**) crystallizes in the triclinic system, space group $P\bar{1}$. Each Y^{3+} is eight coordinated in a bi-augmented trigonal prism coordination environment, defined by six oxygen atoms from five different $hbdc^{2-}$ ligand and two oxygen atoms from two coordination water molecules (Figure 9). On one hand, the $hbdc^{2-}$ ligand connects two independent Y^{3+} ions through bidentate carboxylate groups which leads to 11.4519(9) Å Y-Y distance. On the other hand, four independent Y^{3+} ions are bridged by four oxygen atoms from the carboxylate groups of a ligand which leads to 4.7603(5) Å and 10.0102(8) Å Y-Y distances.

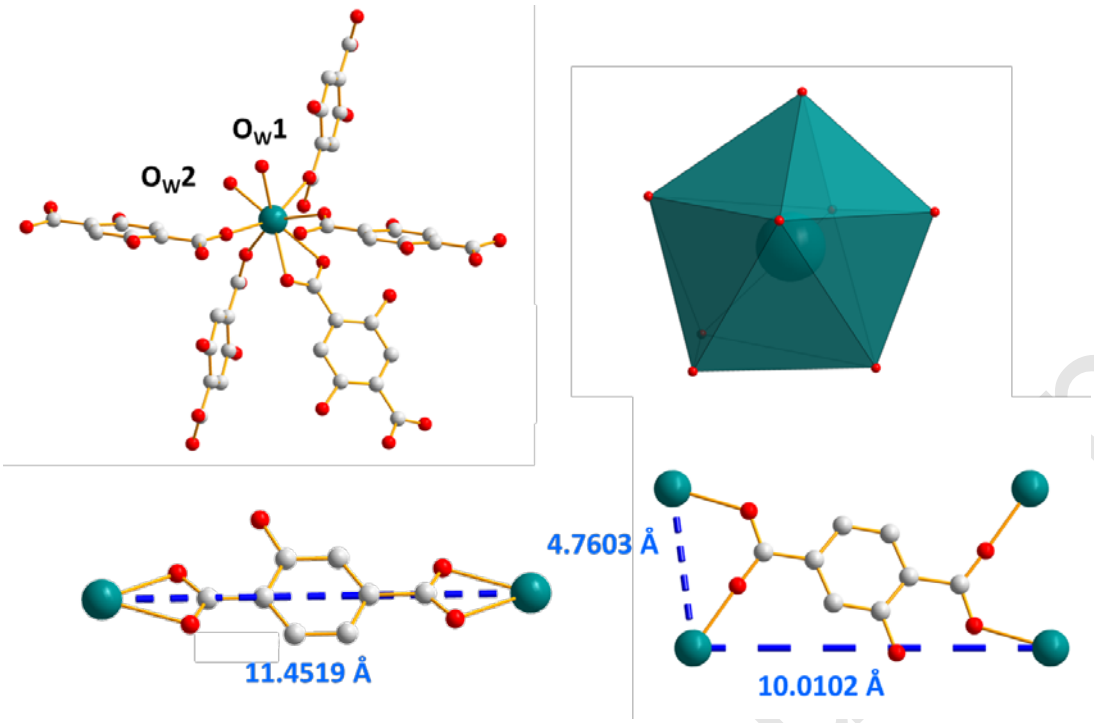

Figure 9. Coordination environment (top left) and coordination polyhedron (top right) of Y^{3+} ions in $[Y_2(hbdc)_3(H_2O)_4{\cdot}4H_2O]_\infty$ (**F3**). The two different coordination modes with Y-Y distances (bottom).

The closest Y^{3+} ions are bridged by one of the carboxylate groups of the ligand that adopts the second coordination mode to form molecular chains that spread along the *a*-axis. These molecular chains are bound to each other through the connection of the other carboxylate groups of the ligands that adopt the second coordination mode. This coordination mode generates a 3-dimensionnal network with 10 x 10 $Å^2$ square cross-section channels. At last, these square cross-section channels are divided into two halves by ligands that adopt the first coordination mode (Figure 10). There are four coordination water molecules and four crystallization water molecules per formula unit (Figure S16). It can be noticed that these compounds are isomorphous to compounds with general chemical formula $[Ln_{1.5}(abdc)_2{\cdot}2H_2O]_\infty$ with Ln = Nd, Eu, Tb, Dy and Y ($abdc^{2-}$ stands for 2-amino-terephthalate) that have been reported previously.[28-31]

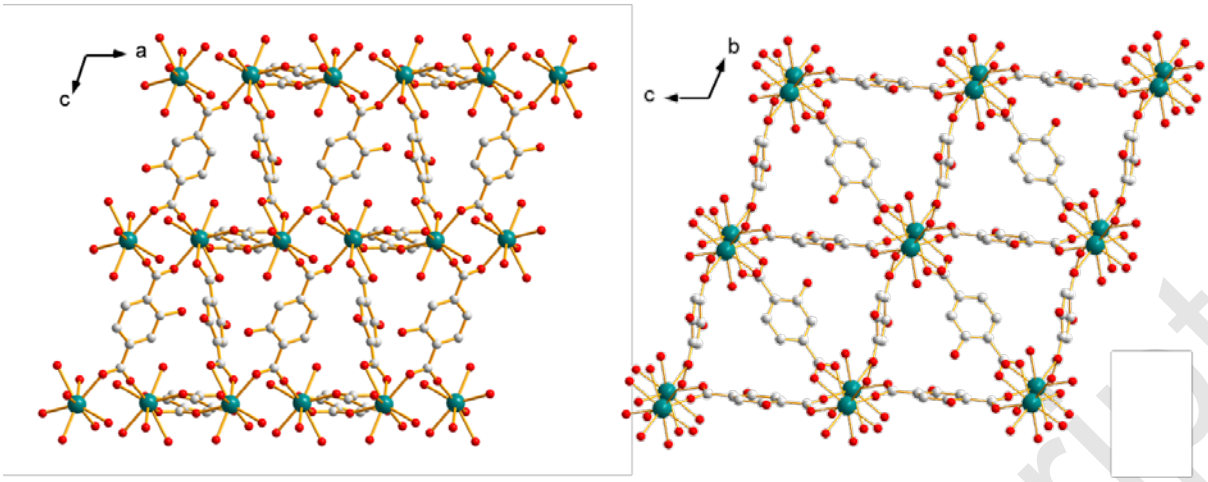

Figure 10. Projection views along the *b*- (left) and *a*-axis (right) of $[Y_2(hbdc)_3(H_2O)_4{\cdot}4H_2O]_\infty$ (**F3**).

Absorption, excitation and emission spectra of $[Gd_2(hbdc)_3(H_2O)_4{\cdot}4H_2O]_\infty$ (**F3**) have been recorded at room temperature (Figure S17 left for absorption) and at room temperature and at 77 K (Figure S17 right for exc/em), in order to estimate the energy of the first excited singlet and triplet states. These measurements shows that $\Delta E(^1\pi^* \leftarrow ^1\pi) = 24390\ cm^{-1}$ and $\Delta E(^3\pi^* \leftarrow ^1\pi) = 27400\ cm^{-1}$. Luminescence decay curve of $[Gd_2(hbdc)_3(H_2O)_4{\cdot}4H_2O]_\infty$ (**F3**) has been recorded at 77 K as well (Figure S18).

Room temperature solid-state excitation and emission spectra as well as luminescence decay curves were recorded for the Eu^{3+}- and the Tb^{3+}-based compounds (Figures 11 and S19). The excitation spectrum of the Tb-derivative shows a broad band that correspond to the ligand $^1\pi^*/^3\pi^* \leftarrow ^1\pi$ transitions. This indicates that the ligands present an efficient antenna effect toward Tb^{3+} ions. On the opposite, because of a PET mechanism, there is no antenna effect toward Eu^{3+} ions. Room temperature solid-state emission spectra have also been measured on the Ho- and Tm- derivatives and show emission in both the visible (centered at 650 nm for Ho or 648 and 780 nm for Tm) and infrared domains (976 for Ho or 1175 nm for Tm) (Figure 11). For the Yb- based compounds the infrared emission at 980 nm has been observed with a good antenna effect.

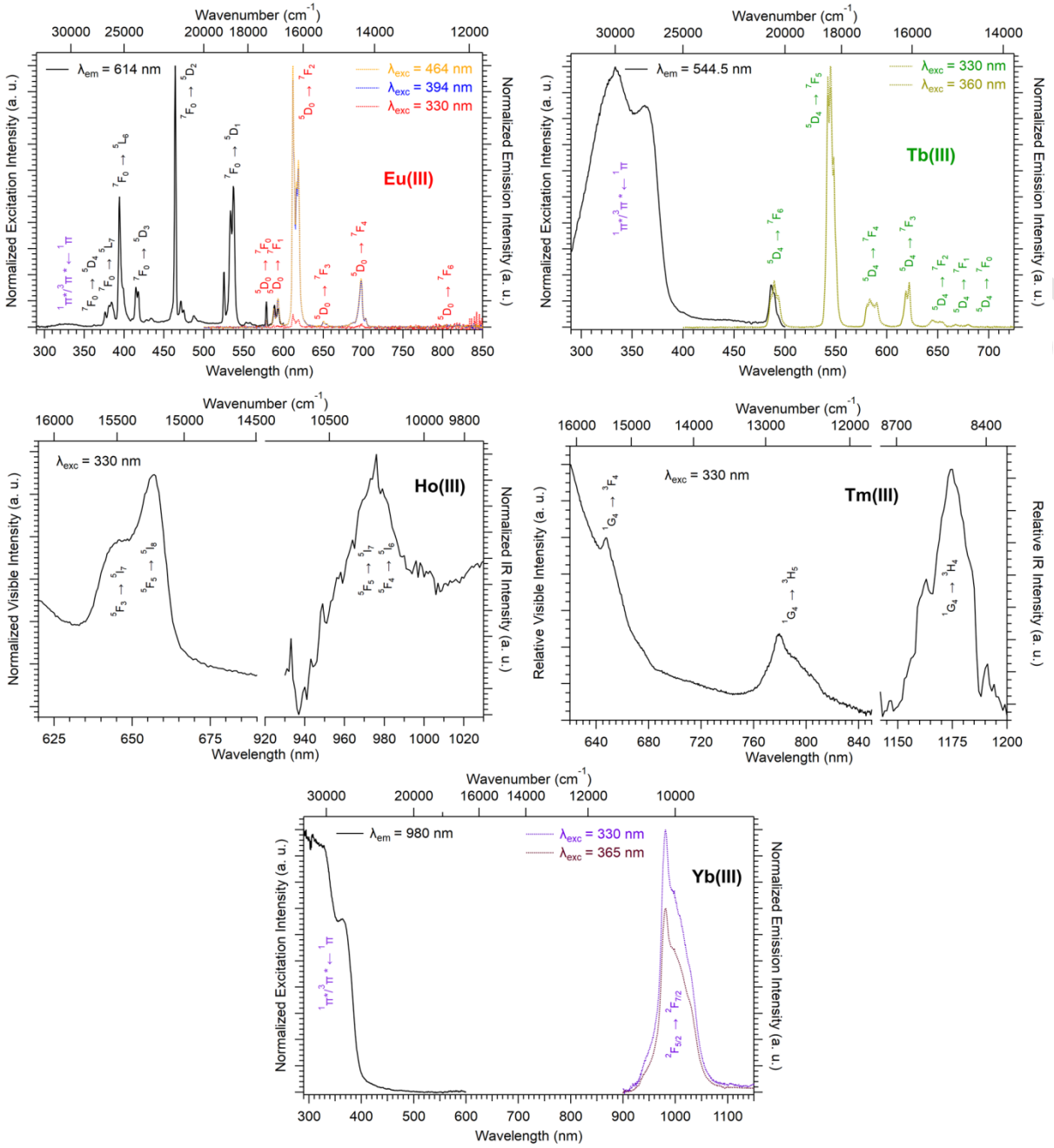

Figure 11. Room temperature solid-state excitation and emission spectra of $[Eu_2(hbdc)_3(H_2O)_4{\cdot}4H_2O]_\infty$ (top left), $[Tb_2(hbdc)_3(H_2O)_4{\cdot}4H_2O]_\infty$ (top right), $[Ho_2(hbdc)_3(H_2O)_4{\cdot}4H_2O]_\infty$ (middle left), $[Tm_2(hbdc)_3(H_2O)_4{\cdot}4H_2O]_\infty$ (middle right) and $[Yb_2(hbdc)_3(H_2O)_4{\cdot}4H_2O]_\infty$ (bottom) (**F3**). τ_{Eu} = 0.29(1) ms and Φ^{Eu}_{Eu} = 14(2)% with λ_{ex} = 394 nm. τ_{Tb} = 0.32(1) ms with λ_{ex} = 330 nm.

Family F4: $[Tb(Hhbdc)(hbdc)(H_2O)_3{\cdot}H_2O]_\infty$

Isostructural Tb^{3+}- and Dy^{3+}-derivatives with chemical formula $[Ln(Hhbdc)(hbdc)(H_2O)_3{\cdot}H_2O]_\infty$ (**F4**) with Ln = Tb-Dy have been obtained by solvothermal

method. Their crystal structure is described on the basis of the Tb^{3+}-derivative: $[Tb(Hhbdc)(hbdc)(H_2O)_3{\cdot}H_2O]_\infty$ crystallizes in the triclinic system, space group $P\bar{1}$. The Tb^{3+} ion is nine coordinated by six oxygen atoms from four different ligands and three oxygen atoms from three coordination water molecules that lead to a spherical capped square antiprism geometry (Figure 12). IR spectrum evidences that, as well as the crystal structure of family **F1**, one of the ligand is once protonated (Figure S20). There are three different coordination modes of the ligands in the crystal structure. In the first one, four different Tb^{3+} ions are connected by two tridentate carboxylate groups of the $hbdc^{2-}$ ligand. In the second, bidentate carboxylate groups of the $hbdc^{2-}$ ligand bridge two different Tb^{3+} ions. In the third, one carboxylate group is bound to one Tb^{3+}. The other carboxylic group is protonated. (Figure 12).

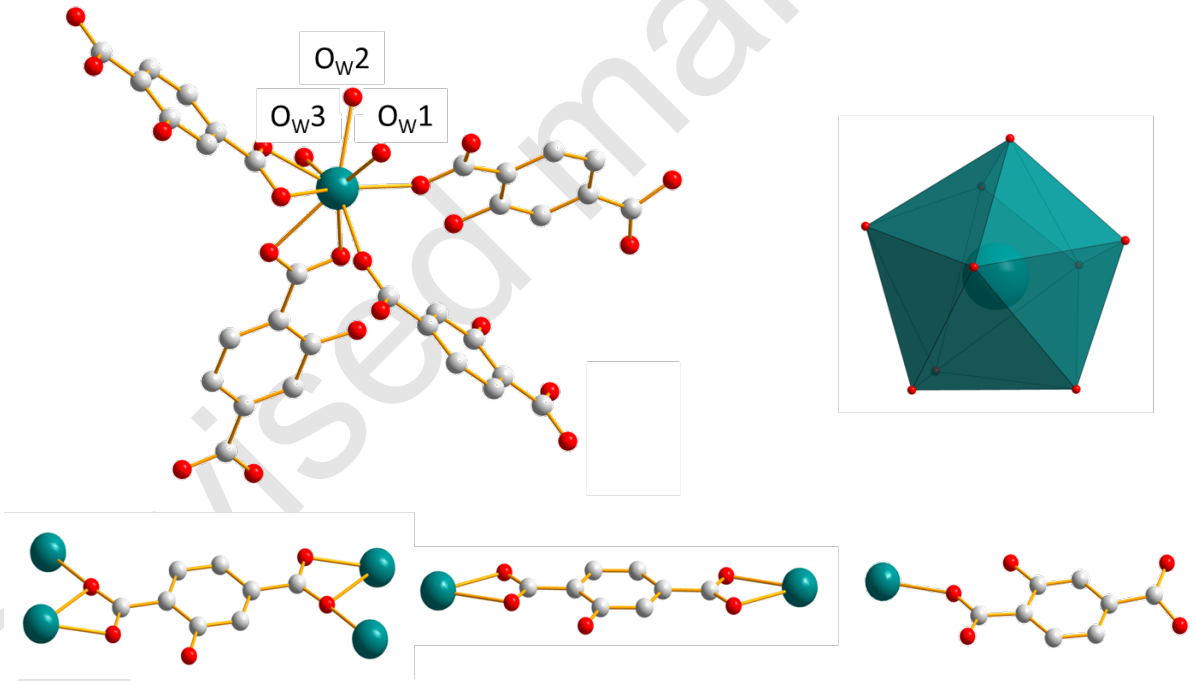

Figure 12. Top: Coordination environment (left) and coordination polyhedron (right) of Tb^{3+} ions in $[Tb(Hhbdc)(hbdc)(H_2O)_3{\cdot}H_2O]_\infty$ (**F4**). Bottom: The three different coordination modes adopted by the ligands in $[Tb(Hhbdc)(hbdc)(H_2O)_3{\cdot}H_2O]_\infty$ (**F4**)

The crystal structure can be described on the basis of 2-dimensional molecular layers that spread parallel to the (*bc*) plane (Figure 13). The Tb-Tb distance in the bi-nuclear units

generated by the first coordination mode is 4.3496(4) Å. The Tb-Tb distance between metallic ions that belong to adjacent bi-nuclear units and that are connected by ligand that adopt the first coordination mode (along the *b*-axis) is 11.6195(9) Å and the distance between lanthanide ions that are connected via the second coordination mode is 11.5109(9) Å (parallel to the *a*-axis). Shortest inter-metallic distance between lanthanide ions that belong to different molecular layers is 7.4407(6) Å.

As confirmed by thermal analyses, there are three coordination water molecules and one crystallization water molecule per formula unit in this crystal structure (Figure S21).

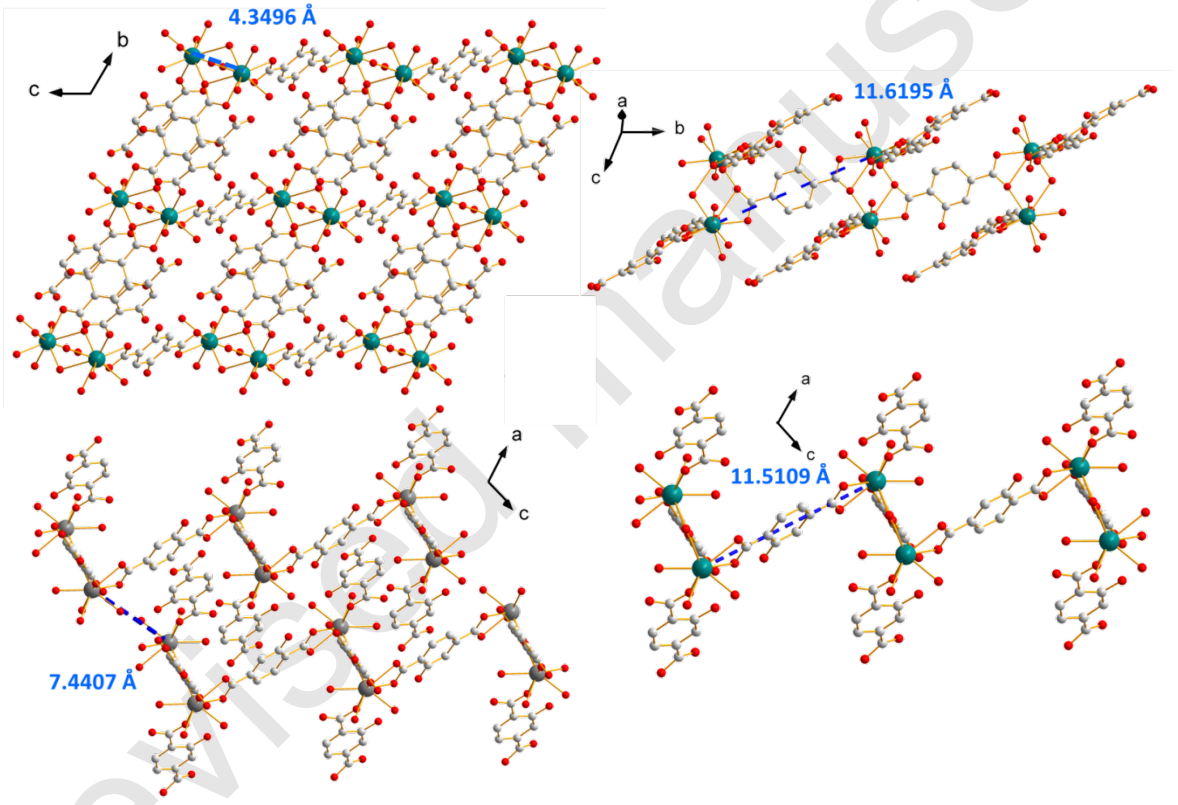

Figure 13. Projection view of a 2-dimensional molecular framework (top left). Projection views that highlight the different Tb-Tb distances in $[Tb(Hhbdc)(hbdc)(H_2O)_3{\cdot}H_2O]_\infty$ (**F4**).

Solid-state excitation and emission spectra were recorded, at room temperature, for both the Tb^{3+}- and the Dy^{3+}-based compounds of family **F4** (Figure 14). Both excitation spectra exhibit two broad bands assigned to the $^1\pi^*/^3\pi^* \leftarrow {}^1\pi$ transitions of the ligand centered at 330 nm and 377 nm, respectively which indicate that the ligand presents an

efficient antenna effect toward both lanthanide ions. The Dy^{3+}-derivative emission can be observed in both the visible and the NIR regions under 330 nm excitation wavelength. Luminescence decay curve of the Tb^{3+}-derivative has been recorded at room temperature as well (Figure S22).

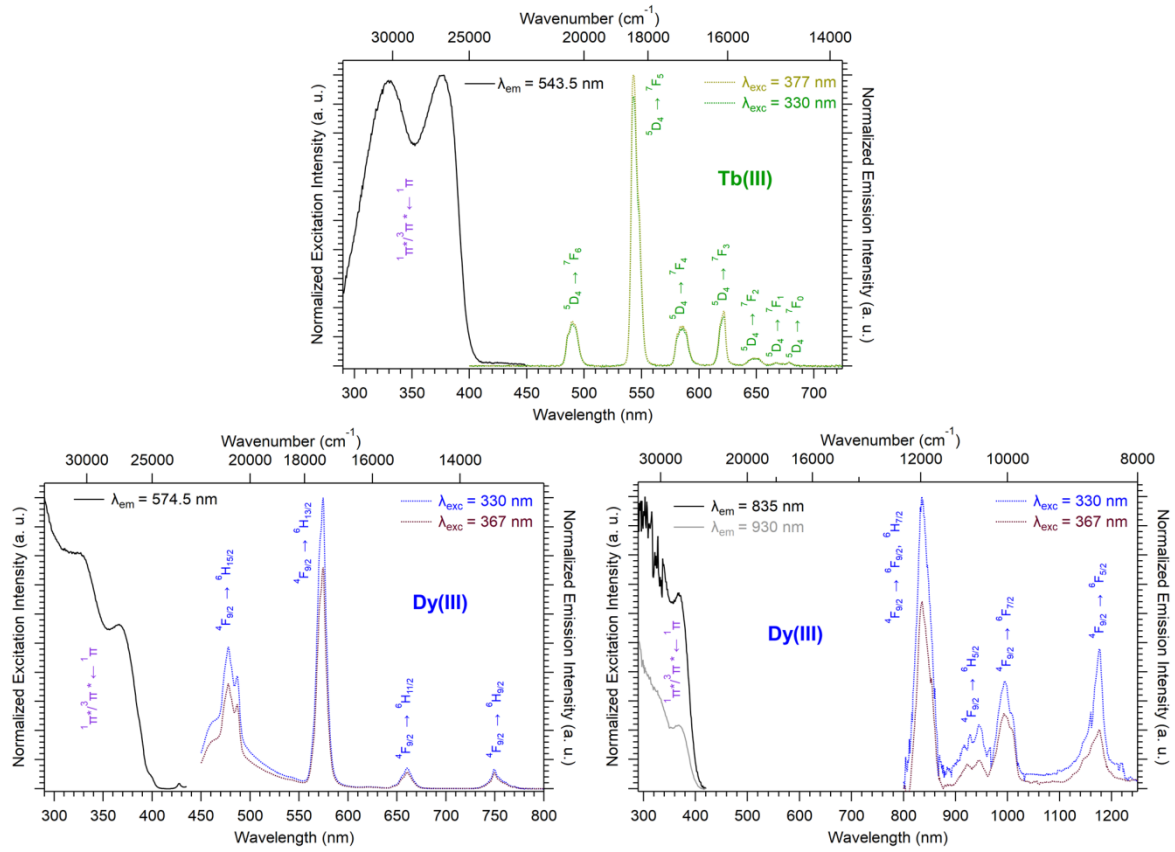

Figure 14. Solid-state excitation and emission spectra of $[Ln(Hhbdc)(hbdc)(H_2O)_3{\cdot}H_2O]_\infty$ (Ln = Tb, Dy) (**F4**) at room temperature. τ_{Tb} = 0.51(1) ms and Φ^{Lig}_{Tb} = 55(2)% with λ_{ex} = 377 nm. Φ^{Lig}_{Dy} = 0.74(1)% with λ_{ex} = 330 nm.

Family F5. $[Gd_2(hbdc)_3(H_2O)_8{\cdot}6H_2O]_\infty$

$[Gd_2(hbdc)_3(H_2O)_8{\cdot}6H_2O]_\infty$, that has been obtained by slow evaporation, crystallizes in the monoclinic system, space group *C*2/*c*. The asymmetric unit contains two Gd^{3+} ions, three $hbdc^{2-}$ ligands, eight coordination water molecules and six crystallization water molecules (Figure S23). Each Gd^{3+} is coordinated by nine oxygen atoms: five from the carboxylate

groups of the ligands and four from coordination water molecules. The coordination polyhedron is best described by the muffin geometry (Figure 15).

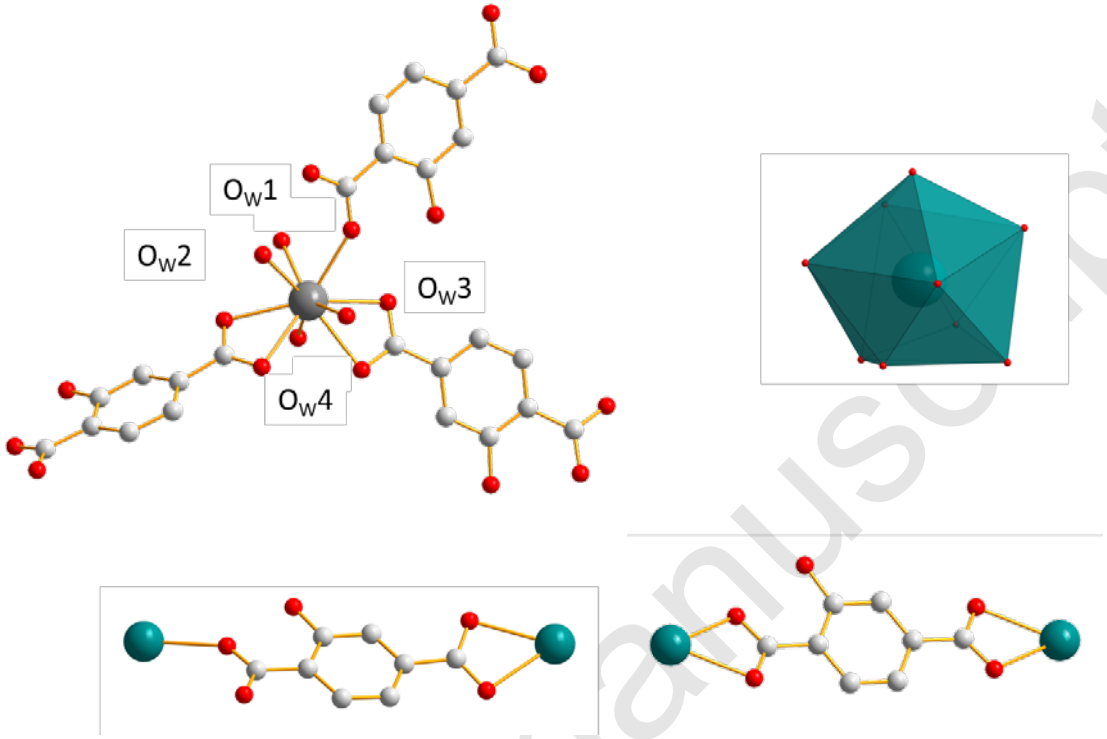

Figure 15. Coordination environment (top left) and coordination polyhedron (top right) of the Gd^{3+} ion and the two different coordination modes of $hbdc^{2-}$ ligand (bottom) in $[Gd_2(hbdc)_3(H_2O)_8{\cdot}6H_2O]_\infty$ (**F5**).

The ligand presents two different coordination modes. In the first one, $hbdc^{2-}$ ligand coordinates two Gd^{3+} ions through monodentate and bidentate carboxylate groups, respectively. In the second one, two Gd^{3+} ions are bridged by bidentate carboxylate groups on both side of the $hbdc^{2-}$ ligand. Six nearby Gd^{3+} ions are connected by six different carboxylate groups with two different coordination modes forming a 2D honeycomb-like molecular layer that spread parallel to the (*ab*) plane (Figure 16). The area of the hexagons is 19 x 11 $Å^2$. The Gd-Gd shortest distances are about 11.5(1) Å.

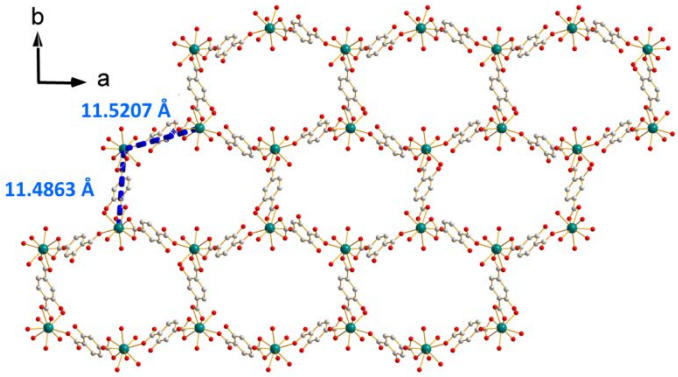

Figure 16. Projection view along the *c*-axis of a 2D honeycomb-like molecular layer of $[Gd_2(hbdc)_3(H_2O)_8{\cdot}6H_2O]_\infty$ (**F5**). Gd-Gd distances are indicated.

The crystal packing can be described as two-fold interpenetrating layers (Figure 17). The shortest Gd-Gd distance between adjacent interpenetrating layers is 5.919(1) Å. The crystallization water molecules are localized in the cavities and bound to the molecular skeleton by hydrogen-bonds that insure the crystal structure stability.

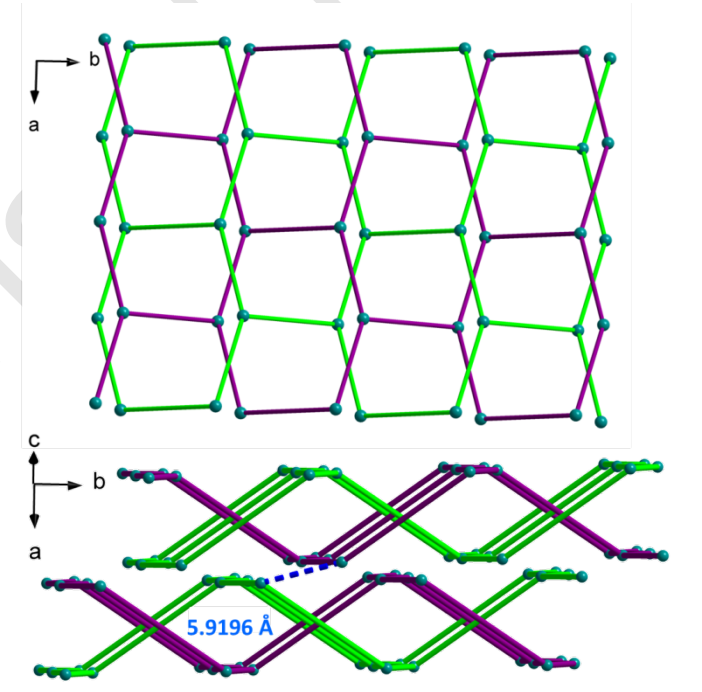

Figure 17. Schematic (ligands are symbolized by a single bar) projection views of two-fold interpenetrating layers in $[Gd_2(hbdc)_3(H_2O)_8{\cdot}6H_2O]_\infty$ (**F5**) (top): the green and purple colors

represent two different interpenetrating layers; Packing mode of the two fold interpenetrating layers with the shortest Gd-Gd distance (bottom)

Solid-state absorption, excitation and emission spectra of $[Gd_2(hbdc)_3(H_2O)_8{\cdot}6H_2O]_\infty$ (**F5**) have been recorded at room temperature (Figure S24 left) and room temperature and 77 K (Figure S24 right), respectively. These spectra allow the estimation of the first excited singlet and triplet state of the ligand.[32] The energy of first excited singlet state of the ligand ($^1\pi^*$) can be estimated by the lowest energy-edge of the UV-absorption spectrum of the Gd^{3+} compounds (~ 26000 cm^{-1}). The energy of the first excited triplet state ($^3\pi^*$) can be assumed by highest energy edge of the emission spectrum of the Gd^{3+} compounds at 77 K (~ 25000 cm^{-1}).

Family F6. $[Gd_2(hbdc)_3(H_2O)_8{\cdot}2H_2O]_\infty$

Compounds that constitute this structural family have chemical formula $[Ln_2(hbdc)_3(H_2O)_8{\cdot}2H_2O]_\infty$ with Ln = Nd-Tb (**F6**). They have been obtained by slow diffusion through gel media. The coordination environment of $[Gd_2(hbdc)_3(H_2O)_8{\cdot}2H_2O]_\infty$ (**F6**) is similar to that of $[Gd_2(hbdc)_3(H_2O)_8{\cdot}6H_2O]_\infty$ (**F5**). In both crystal structures, each Gd^{3+} ion is coordinated by nine oxygen atoms from three different ligands and four coordination water molecules (Figure 18) and the coordination geometry is best described as muffin geometry. In structural type **F6**, the $hbdc^{2-}$ ligand adopts two different coordination modes (Figure 18). In the first coordination mode, both carboxylate groups bridge one Gd^{3+} ion in a monodentate way. In the second one, bidentate carboxylate groups connect one Gd^{3+} ion on both sides.

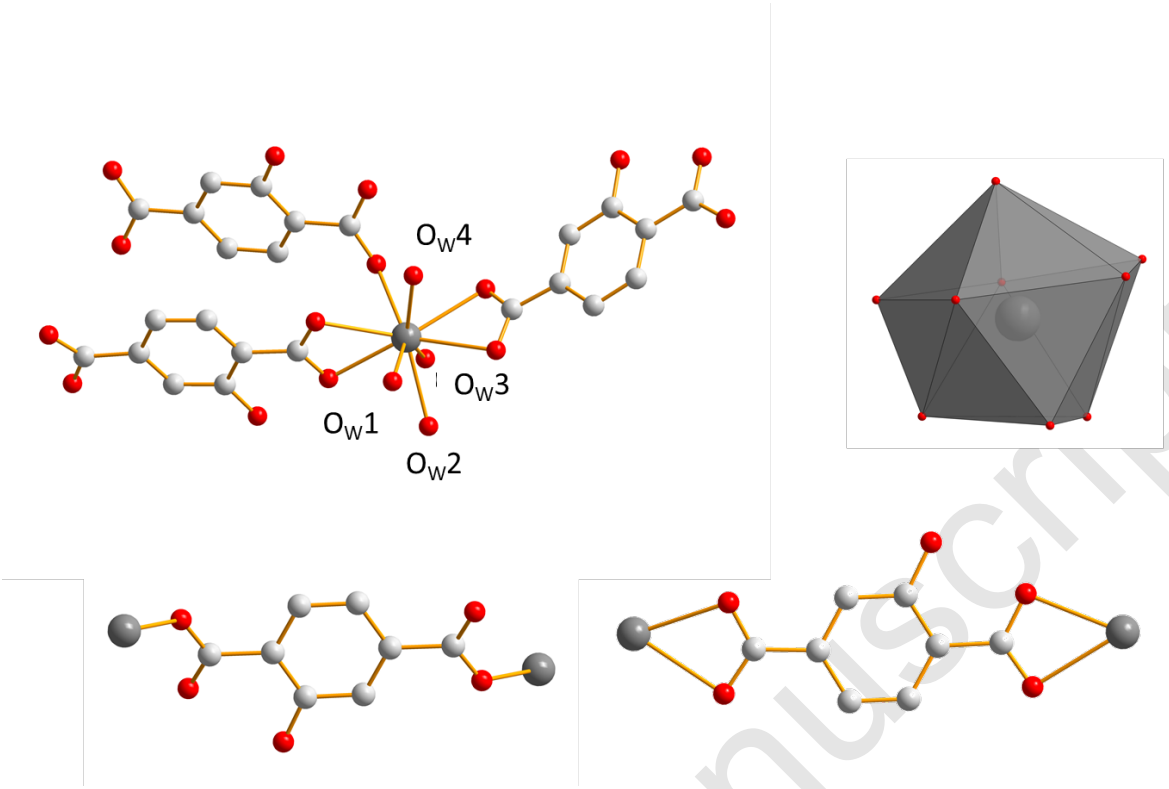

Figure 18. Coordination environment (top left), coordination polyhedron (top right) of Gd^{3+} ions and the two coordination modes (bottom) of $hbdc^{2-}$ ligand in $[Gd_2(hbdc)_3(H_2O)_8{\cdot}2H_2O]_\infty$ (**F6**).

The crystal structure can be described on the basis of 2-dimensional molecular layers made of hexa-nuclear rings (Figure 19). Two different Gd-Gd distances with two different coordination modes of the ligand can be observed in these rings: 11.0526(11) Å and 11.3667(13) Å. Compared with those observed in the crystal structure of **F5**, the hexa-nuclear rings are smaller and narrower. Their area is 15 x 5 $Å^2$. This can be related to the fact that there are only two crystallization water molecules per formula unit in $[Gd_2(hbdc)_3(H_2O)_8{\cdot}2H_2O]_\infty$ (**F6**) instead of six in $[Gd_2(hbdc)_3(H_2O)_8{\cdot}6H_2O]_\infty$ (**F5**) (Figure S25). The 2-dimensional molecular layers can be described as wrapped planes made of cyclohexane-like rings (Figure 20).

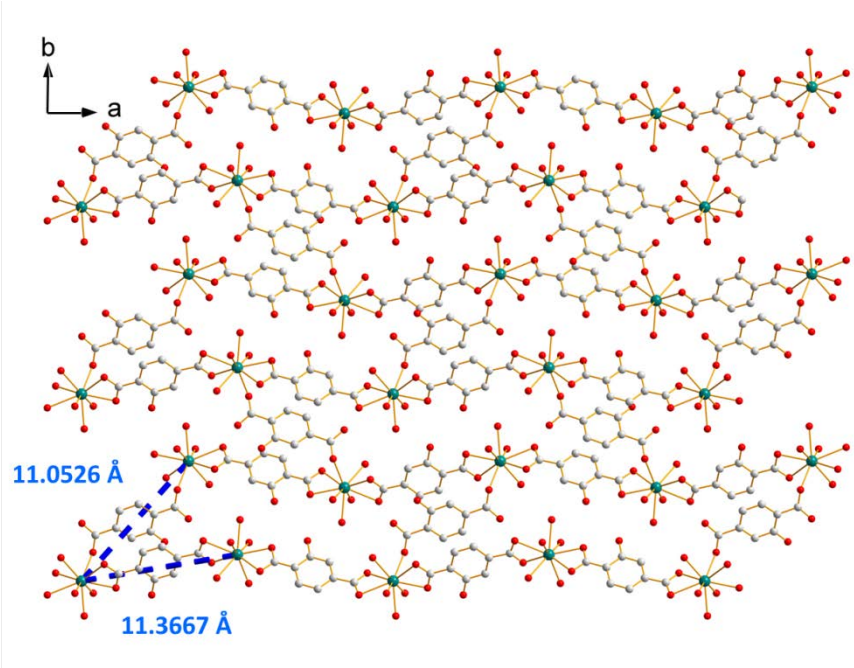

Figure 19. Projection view along the *c*-axis of a 2-dimensional molecular layer in $[Gd_2(hbdc)_3(H_2O)_8{\cdot}2H_2O]_\infty$ (**F6**) with shortest Gd-Gd distances.

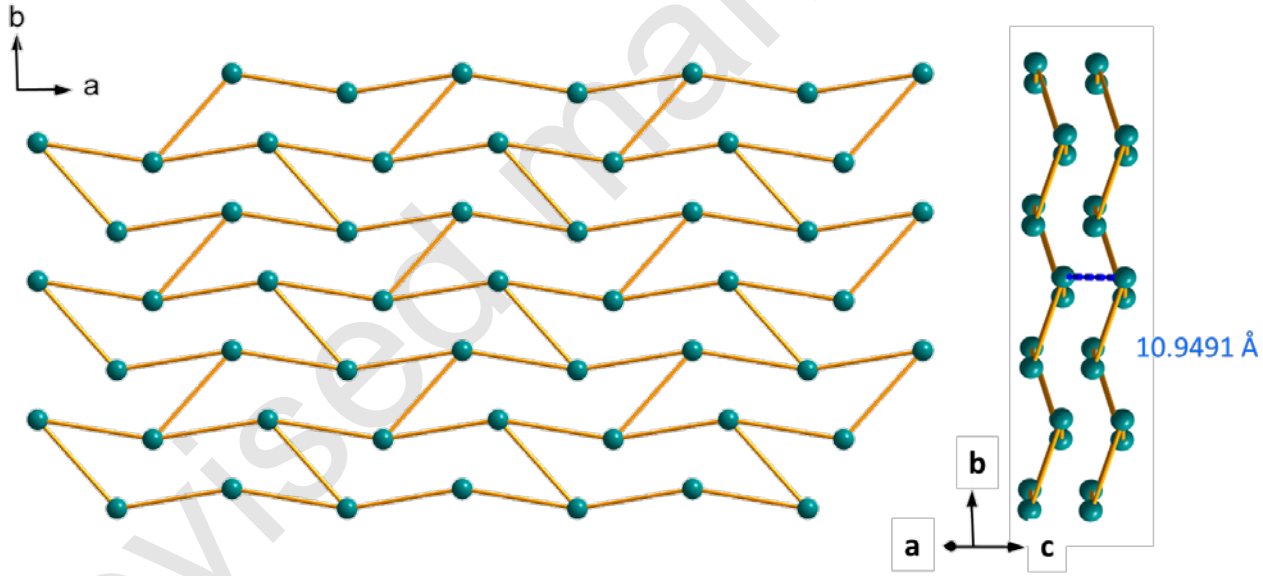

Figure 20. Schematic (bars symbolize the ligands) projection view along the *c*-axis (left) and packing of the molecular layers (right) of $[Gd_2(hbdc)_3(H_2O)_8{\cdot}2H_2O]_\infty$ (**F6**).

Absorption and emission spectra of $[Gd_2(hbdc)_3(H_2O)_8{\cdot}2H_2O]_\infty$ (**F6**) have been recorded at room temperature and at 77 K, respectively (Figure S26), in order to estimate the energy of the first excited singlet and triplet states. These measurements shows that $\Delta E(^1\pi^* \leftarrow {}^1\pi) \sim 24390\ cm^{-1}$ and $\Delta E(^3\pi^* \leftarrow {}^1\pi) \sim 25000\ cm^{-1}$.

Room temperature solid-state excitation and emission spectra have been recorded for the Nd^{3+}- and Tb^{3+}-derivatives of family **F6** (Figure 21). Excitation spectra of both compounds exhibit two broad bands centered at 325 nm and 360 nm strongly suggesting an efficient antenna effect of the ligand toward both lanthanide ions. Luminescence decay curve of the Tb-derivative has been recorded at room temperature as well (Figure S27).

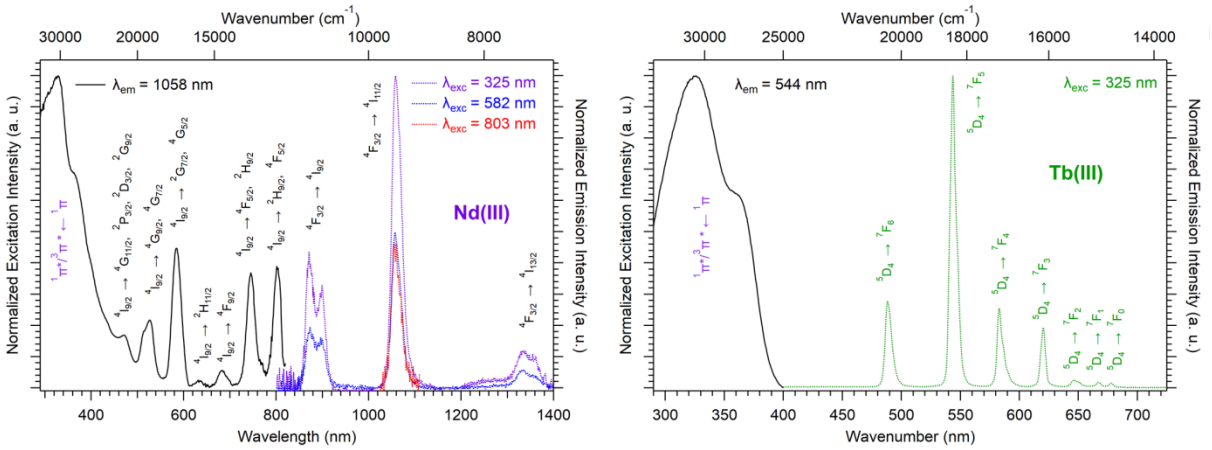

Figure 21. Solid-state excitation and emission spectra of $[Nd_2(hbdc)_3(H_2O)_8{\cdot}2H_2O]_\infty$ (**F6**) (left) and $[Tb_2(hbdc)_3(H_2O)_8{\cdot}2H_2O]_\infty$ (**F6**) (right) at room temperature. τ_{Tb} = 0.63(1) ms and Φ^{Lig}_{Tb} = 36(1)% with λ_{ex} = 325 nm.

Luminescent properties of the hetero-lanthanide compounds: $[Tb_{2x}Eu_{2-2x}(hbdc)_3(H_2O)_8{\cdot}6H_2O]_\infty$ (F5) and $[Tb_{2x}Eu_{2-2x}(hbdc)_3(H_2O)_8{\cdot}2H_2O]_\infty$ (F6) ($0 < x < 1$).

Because Tb^{3+}- and Eu^{3+}-derivatives usually present interesting luminescent properties in the visible domain, we have prepared hetero-lanthanide Tb^{3+}/Eu^{3+}compounds for investigating the inter-metallic energy transfers and modulating the emission color. In this system, whatever the crystal structures of the microcrystalline powders of the homo-Tb^{3+} and Eu^{3+}-derivatives are, the microcrystalline powders of the Tb^{3+}/Eu^{3+} hetero-lanthanide compounds always crystallize in the crystal structure of the Gd^{3+}-derivatives (**F5** or **F6**). For the microcrystalline powder of the Gd^{3+}-derivative, the crystal structure depends on the order of addition of the reactants: adding the solution of gadolinium chloride into the solution of

Na_2hbdc leads to $[Gd_2(hbdc)_3(H_2O)_8{\cdot}6H_2O]_\infty$ (**F5**). On the contrary, $[Gd_2(hbdc)_3(H_2O)_8{\cdot}2H_2O]_\infty$ (**F6**) is obtained when the solution of Na_2hbdc is added to the gadolinium chloride solution. The same happens for Tb^{3+}/Eu^{3+} mixtures.

This phenomenon provides a platform to synthesize two different series of Tb^{3+}/Eu^{3+} hetero-lanthanide compounds with respective chemical formulas $[Tb_{2x}Eu_{2-2x}(hbdc)_3(H_2O)_8{\cdot}6H_2O]_\infty$ (**F5**) and $[Tb_{2x}Eu_{2-2x}(hbdc)_3(H_2O)_8{\cdot}2H_2O]_\infty$ (**F6**) ($0 < x < 0.9$).

Solid-state emission spectra of the two series of Tb^{3+}/Eu^{3+} hetero-lanthanide compounds are reported in Figure 22 and Figure 23. Corresponding colorimetric coordinates have also been calculated on the basis of the emission spectra.

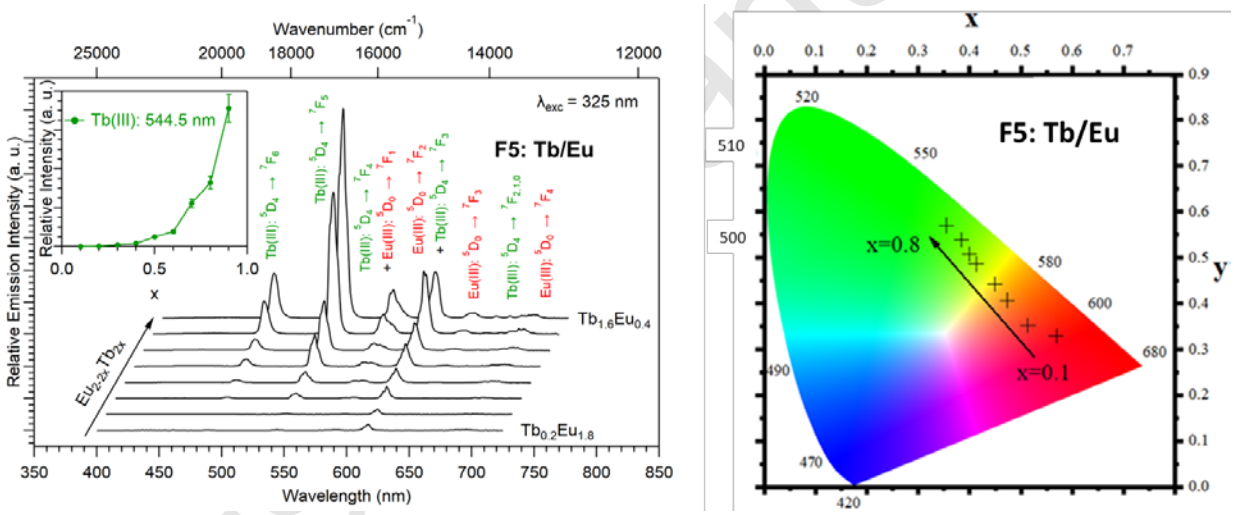

Figure 22. Solid-state emission spectra (left) and corresponding colorimetric coordinates (right) of$[Tb_{2x}Eu_{2-2x}(hbdc)_3(H_2O)_8{\cdot}6H_2O]_\infty$ (**F5**) ($0 < x < 0.8$) *versus* x under 325 nm excitation wavelength at room temperature. In inset: relative intensity (between 0 and 1) of the major emission peak of Tb^{3+} ions *versus* x.

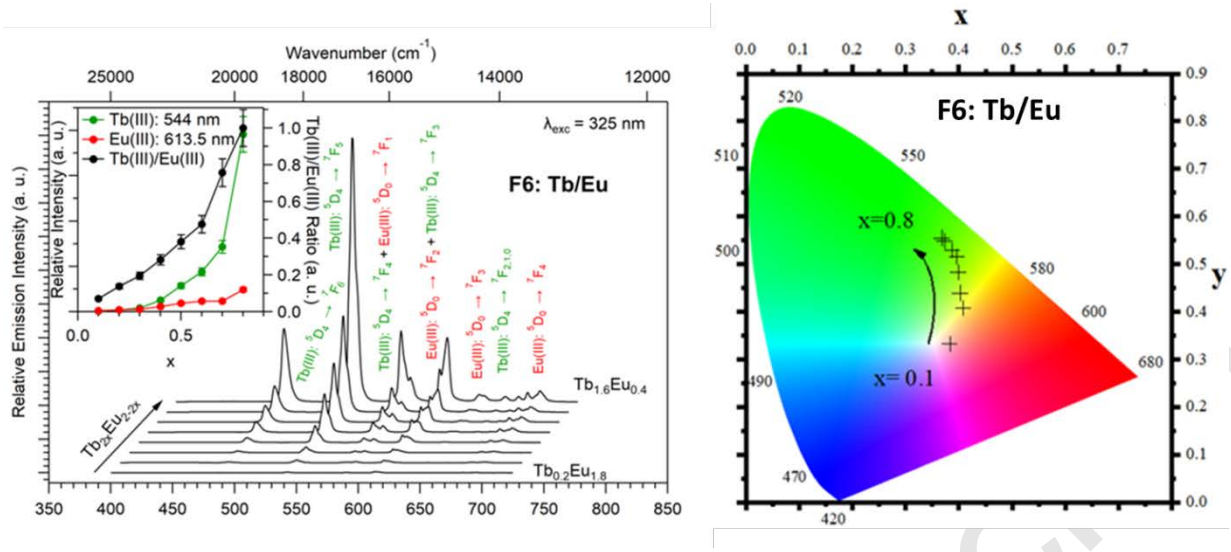

Figure 23. Solid-state emission spectra (left) and corresponding colorimetric coordinates (right) of $[Tb_{2x}Eu_{2-2x}(hbdc)_3(H_2O)_8{\cdot}2H_2O]_\infty$ (**F6**) ($0 < x < 0.8$) *versus* x under 325 nm excitation wavelength at room temperature. In inset: relative intensities (between 0 and 1) of the major emission peaks of Tb^{3+} and Eu^{3+} ions *versus* x as well as their ratio.

For both series of compounds, emission spectra show the characteristic emission peaks of Tb^{3+} and Eu^{3+} ions. In both cases the increase of the Tb^{3+}concentration provokes an increasing of the luminescence intensity of the Tb^{3+} ions and of that of the Eu^{3+} ions as well. This strongly suggests Tb-to-Eu inter-metallic energy transfers. However, inter-metallic energy transfer processes are different in the two series of compounds: For $[Tb_{2x}Eu_{2-2x}(hbdc)_3(H_2O)_8{\cdot}6H_2O]_\infty$ (**F5**), the emission color progressively changes from red to orange to yellow to green whereas for $[Tb_{2x}Eu_{2-2x}(hbdc)_3(H_2O)_8{\cdot}2H_2O]_\infty$ (**F6**), the emission color directly changes from orange to yellow then green. Indeed, with the same Tb^{3+} content ($x = 0.1$), the emission color of the compound that belongs to **F5** is in the red region, and in the orange region for the compound that belongs to **F6**.

In order to further compare these two series of compounds, we have measured the luminance under UV irradiation for both series of compounds (Figure 24).

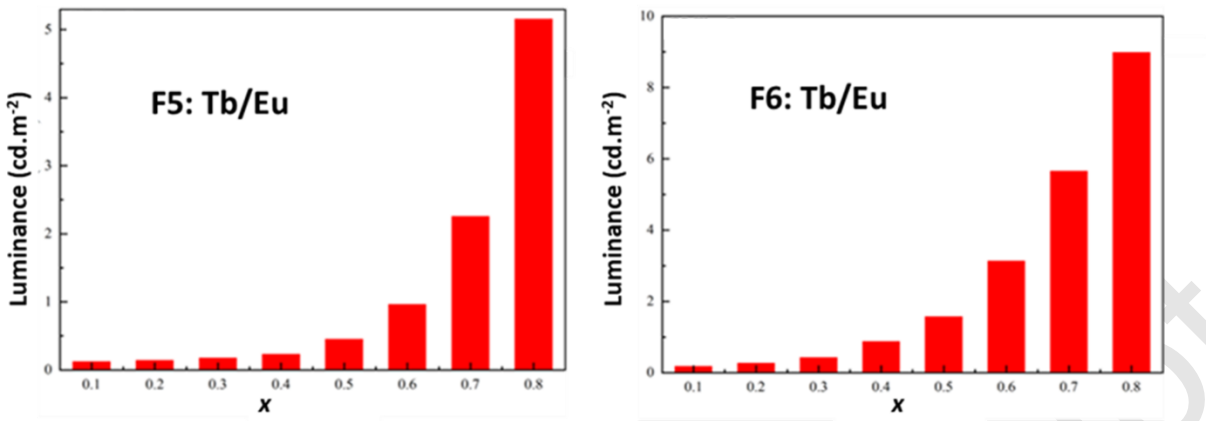

Figure 24. Luminance *versus* *x* (right) of $[Tb_{2x}Eu_{2-2x}(hbdc)_3(H_2O)_8{\cdot}6H_2O]_\infty$ (**F5**) (left) and $[Tb_{2x}Eu_{2-2x}(hbdc)_3(H_2O)_8{\cdot}2H_2O]_\infty$ (**F6**) (right) under UV irradiation (flux 0.68(1) $mW.cm^{-2}$; λ_{exc} = 312 nm).

Figures 22 to 24 show that the two series present quite different behaviors versus *x* and suggest that inter-metallic energy transfers are more efficient in **F5** than in **F6**. Excited singlet and triplet energy levels of the ligand are essentially identical (Figures S24 and S26) and therefore cannot be responsible of the discrepancy between the optical behaviors.

From the point of view of their crystal structure these compounds are close to each other: both present eight coordination water molecules per formula unit, the coordination polyhedrons of the lanthanide ions are similar and both crystal structures can be described on the basis of molecular layers made of hexagonal rings. Moreover, intermetallic distances inside a given molecular layer are similar (around 11 Å) and the mean inter-metallic distances estimated with the rough model that have been previously described[33] are almost identical: 12.8 Å and 12.5 Å, respectively. The main difference between the two crystal structures is the packing of the molecular layers. Indeed, the shortest inter-metallic distances between lanthanide ions that belong to different layers is 10.9 Å in **F6** structural type and only 5.9 Å in **F5** one. It has already been shown that this can be of first importance as far as luminescence is concerned.[34]

Dilution effect in F6 structural type: $[Gd_{2x}Eu_{2-2x}(hbdc)_3(H_2O)_8{\cdot}2H_2O]_\infty$ (F6) and $[Gd_{2x}Tb_{2-2x}(hbdc)_3(H_2O)_8{\cdot}2H_2O]_\infty$ (F6) with $0 < x < 1$.

In order to more deeply investigate the unexpected luminescence behavior of the compounds that belong to family **F6** we have synthesize two more series of compounds: $[Gd_{2x}Eu_{2-2x}(hbdc)_3(H_2O)_8{\cdot}2H_2O]_\infty$ (**F6**) and $[Gd_{2x}Tb_{2-2x}(hbdc)_3(H_2O)_8{\cdot}2H_2O]_\infty$ (**F6**) with $0 < x < 1$, by adding the solution of Na_2hbdc to the lanthanide chlorides solution. As expected, all these compounds are isostructural to $[Gd(hbdc)_3(H_2O)_8{\cdot}2H_2O]_\infty$ (**F6**) (Figures S10-S11). Relative metallic contents are gathered in Table S1.

Room temperature solid state emission spectra have been recorded (λ_{exc} = 325 nm) and luminance measurements have been performed (flux 0.68(1) $mW.cm^{-2}$; λ_{exc} = 312 nm) (Figures 25 and S28).

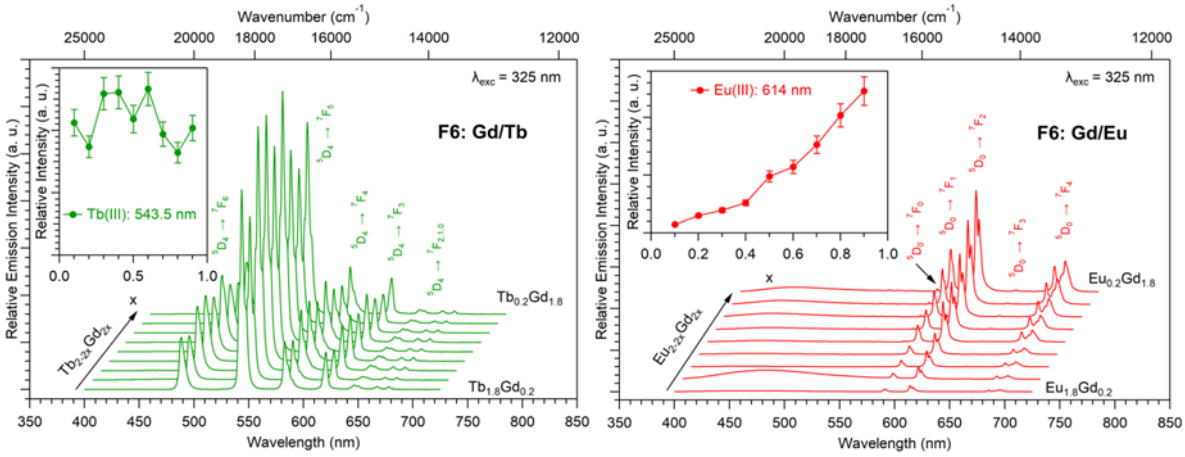

Figure 25. Solid-state emission spectra under UV irradiation (325 nm) of $[Gd_{2x}Tb_{2-2x}(hbdc)_3(H_2O)_8{\cdot}2H_2O]_\infty$ (**F6**) (left) and $[Gd_{2x}Eu_{2-2x}(hbdc)_3(H_2O)_8{\cdot}2H_2O]_\infty$ (**F6**) (right) *versus* x ($0 < x < 1$) at room temperature. In insets: relative intensities (between 0 and 1) of the major emission peaks.

Figures 25 and S28 show that despite big inter-metallic distances, inter-metallic energy transfers are still present in **F6** structural type. Indeed, The luminance of the compounds with chemical formula $[Gd_{2x}Tb_{2-2x}(hbdc)_3(H_2O)_8{\cdot}2H_2O]_\infty$ (**F6**) is almost constant over all the x range whereas in absence of intermetallic energy transfer it is expected to

decrease proportionally to the Tb^{3+} concentration. This was expected because even if it is commonly admitted that 10 Å is the threshold above which inter-metallic energy transfer become less efficient,[35] they are still present at bigger distances. On the contrary, Eu luminescence, under excitation of the ligand, appears and increases as *x* increases. This strongly suggests that dilution by an optically inactive ion (Gd^{3+}) not only reduces inter-metallic energy transfers but also allows the apparition of an antenna effect. This could be related to the number of ligands available for transferring their energy per Eu^{3+} ion that increases upon dilution by Gd^{3+}. This was unexpected and, to the best of our knowledge never observed before for lanthanide based coordination polymers.

Nevertheless, it must be noticed that dilution by an optically inactive lanthanide ion provokes only a weak increasing of the luminance (x 5 for $x = 0.9$ – Figure S24) whereas dilution by a Tb^{3+} ion induces a greater increasing (x 50 for $x = 0.8$ - (Figure 24). This confirms that Tb-to-Eu inter-metallic energy transfers are efficient and feeds the emitting levels of the Eu^{3+} ion. On the basis of this observation we have decided to try to prepare a series of hetero-lanthanide coordination polymers that would present the structural type **F6** and exhibit tunable emission.

Modulation of the luminescence: $[Gd_{1.8}Tb_{0.2x}Eu_{0.2-0.2x}(hbdc)_3(H_2O)_8{\cdot}2H_2O]_\infty$ (F6) ($0 < x < 1$)

In order to observe a sizeable Eu^{3+} emission and to prevent PET, the Gd^{3+} concentration has been set to 90% and relative contents in Eu^{3+} and Tb^{3+} allowed to vary. The prepared compounds have general chemical formula $[Gd_{1.8}Tb_{0.2x}Eu_{0.2-0.2x}(hbdc)_3(H_2O)_8{\cdot}2H_2O]_\infty$ with $0 < x < 1$ and are isostructural to $[Gd_2(hbdc)_3(H_2O)_8{\cdot}2H_2O]_\infty$ (**F6**) (Figure S29 and Table S2). Their emission spectra

(λ_{exc} = 325 nm) have been recorded and their colorimetric coordinates and luminance (λ_{exc} = 312 nm) have been measured (Figure 26).

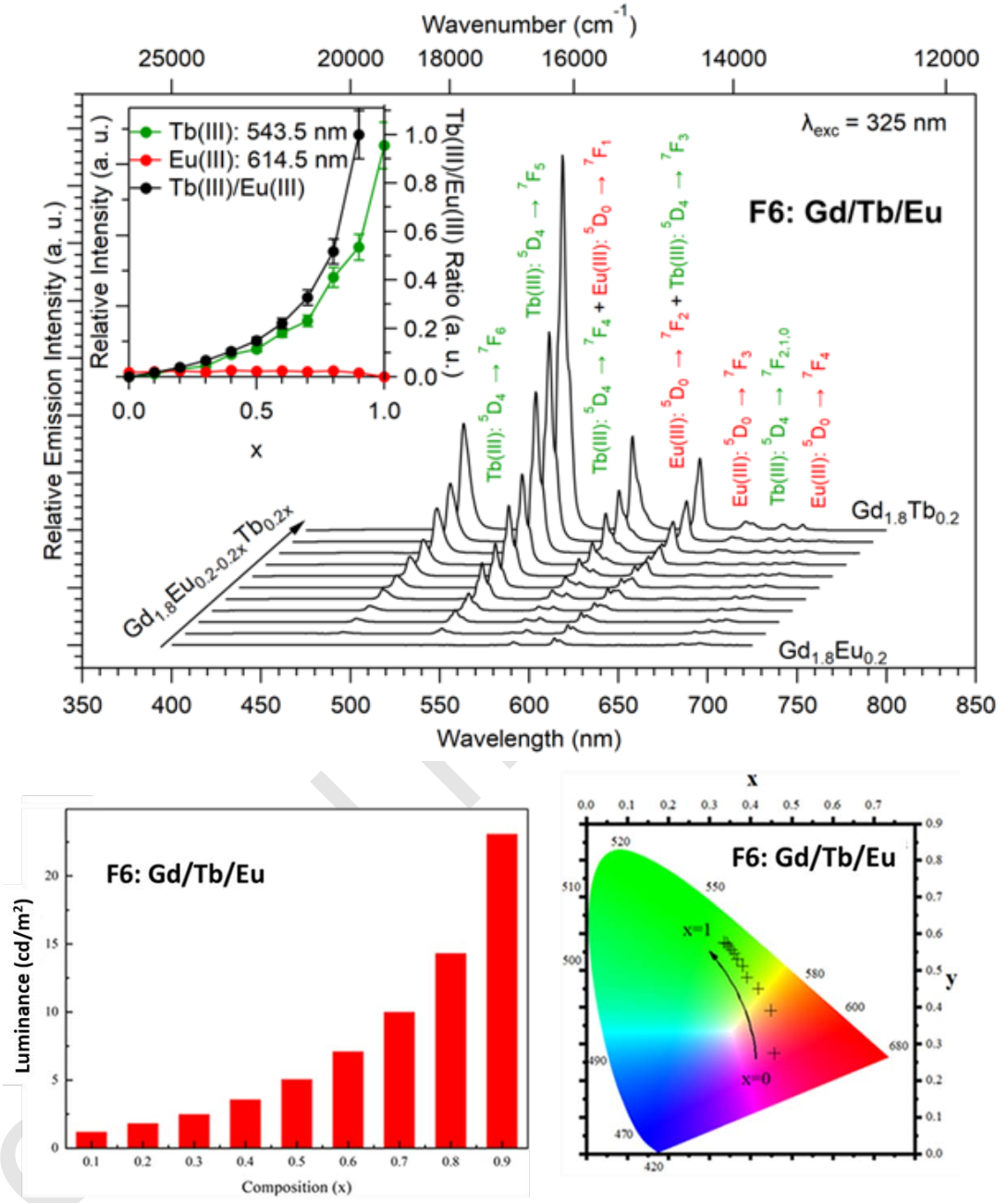

Figure 26. Solid-state emission spectra (top) (λ_{exc} = 325 nm) *versus x*. In inset the intensities of the major emission peaks of Tb^{3+} and Eu^{3+} ions as well as their ratio, *versus x*. colorimetric coordinates (bottom right) (λ_{exc} = 312 nm) and luminance measurements (bottom left) (λ_{exc} = 312 nm) *versus x* of $[Gd_{1.8}Tb_{0.2x}Eu_{0.2-0.2x}(hbdc)_3(H_2O)_8{\cdot}2H_2O]_\infty$ (**F6**) ($0 \le x \le 1$).

Figure 26 evidences that it is possible to design compounds with tunable color emission and brightness. However, even if some of these compounds exhibit emission spectra

that contain a red component despite the presence of the PET mechanism, one must notice that emission color and brightness don't vary independently. Indeed, it is possible to design compounds with quite sizeable luminance that emit in the green region but not in the red region.

CONCLUSION AND OUTLOOK.

Reactions in water between lanthanide chlorides and the di-sodium salt of 2-hydroxy-terephthallic acid have led to six new series of lanthanide-based coordination polymers. It is noticeable that two out of the six crystal structures are isomorphous to 2-amino-terephthallic-based analogues and that the -OH group doesn't participate to lanthanide coordination. This system is very versatile and it is possible to prepare compounds with identical metallic composition and different crystal structures, in similar experimental conditions, just changing the reactants order of addition. As anticipated this ligand induces a very efficient quenching of the Eu^{3+} luminescence because of PET mechanism. However this study evidences that it is possible to overcome this mechanism by dilution by optically inactive ions and to obtained series of compounds with tunable emission color and intensity.

ACKNOWLEDGEMENTS.

The Chinese Scholarship Council is acknowledged for its financial support in the frame of the Chinese-INSA/UT network.

SUPPORTING INFORMATION

Supporting information contains detailed experimental procedure for syntheses of $Na_2(hbdc)\cdot H_2O$ and of the single-crystals of the coordination polymers, for single crystals and powders X-ray diffraction, for thermal analyses, for electron dispersive spectroscopy and for

optical measurements. It also contains additional TG/TD, PXRD, FTIR, EDS and optical measurements.

REFERENCES

1. Cui, Y.; Zhang, J.; He, H.; Qian, G., Photonic functional metal–organic frameworks. *Chem. Soc. Rev.* **2018,** *47*, 5740-5785.
2. Cui, Y.; Li, B.; He, H.; Zhou, W.; Chen, B.; Qian, G., Metal-organic frameworks as platforms for functionnal materials. *Accounts Chem. Res.* **2016,** *49*, 483-493.
3. Cui, Y.; Zhang, J.; Chen, B.; Qian, G., Lanthanide Metal-Organic Frameworks for Luminescent Applications. *Handbook on the Physics and Chemistry of Rare Earths* **2016,** *50*, 243-268.
4. Li, B.; Wen, H.-M.; Cui, Y.; Qian, G.; Chen, B., Multifunctionnal lanthanide coordination polymers. *Prog. Polym. Sci.* **2015,** *48*, 40-84.
5. He, J.; Xu, J.; Yin, J.; Li, N.; Bu, X.-H., Recent advances in luminescent metal-organic frameworks for chemical sensors. *Science China Materials* **2019,** *62*, 1655-1678.
6. Eliseeva, S. V.; Bünzli, J. C. G., Lanthanide luminescence for functionnal materials and bio-sciences. *Chem. Soc. Rev.* **2010,** *39*, 189-227.
7. Bünzli, J.-C. G., Lanthanide luminescence for biomedical analyses and imaging. *Chem. Rev.* **2010,** *111*, 2729-2755.
8. Han, Y.; Yan, P.; Sun, J.; An, G.; Yao, X.; Li, Y.; Li, G., Luminescence and white-light emitting luminescent sensor of tetrafluoroterephthalatelanthanide metal–organic frameworks. *Dalton Trans.* **2017,** *46*, 4642-4653.
9. Bünzli, J. C. G., Rising stars in science and technology : Luminescent lanthanide materials. *Eur. J. Inorg. Chem.* **2017**, 5058-5063.
10. Wang, K.-M.; Du, L.; Ma, Y.-L.; Zhao, J.-S.; Wang, Q.; Yan, T.; Zhao, Q.-H., Multifunctionnal chemical sensors and luminescent thermometers based on lanthanide metal-organic framework materials. *Cryst. Eng. Comm.* **2016,** *18*, 2690-2700.
11. Brites, D. S. C.; Millan, A.; Carlos, L. D., Lanthanides in Luminescent Thermometry. In *Handbook on the Physics and Chemistry of Rare Earths*, Gschneidner, K. A.; Bünzli, J. C. G.; Pecharsky, V. K., Eds. Elsevier: **2016**; Vol. 49, p 339-427.
12. Guillou, O.; Daiguebonne, C.; Calvez, G.; Bernot, K., A long journey in lanthanide chemistry : from fundamental crystallogenesis studies to commercial anti-counterfeiting taggants. *Accounts Chem. Res.* **2016,** *49*, 844-856.
13. Pearson, R. G., Hard and soft acids and bases - the evolution of a chemical concept. *Coord. Chem. Rev.* **1990,** *100*, 403-425.
14. Le Natur, F.; Calvez, G.; Freslon, S.; Daiguebonne, C.; Bernot, K.; Guillou, O., Extending the lanthanide terephthalate system : isolation of an unprecedented Tb(III)-based coordnation polmer with high potential porosity and luminescence properties. *J. Mol. Struc.* **2015,** *1086*, 34-42.
15. Kerbellec, N.; Kustaryono, D.; Haquin, V.; Etienne, M.; Daiguebonne, C.; Guillou, O., An Unprecedented Family of Lanthanide-Containing Coordination Polymers with Highly Tunable Emission Properties. *Inorg. Chem.* **2009,** *48*, 2837-2843.
16. Daiguebonne, C.; Kerbellec, N.; Guillou, O.; Bünzli, J. C. G.; Gumy, F.; Catala, L.; Mallah, T.; Audebrand, N.; Gérault, Y.; Bernot, K.; Calvez, G., Structural and luminescent properties of micro-sized and nano-sized particles of lanthanide terephthalate coordination polymers. *Inorg. Chem.* **2008,** *47*, 3700-3708
17. Freslon, S.; Luo, Y.; Calvez, G.; Daiguebonne, C.; Guillou, O.; Bernot, K.; Michel, V.; Fan, X., Influence of photo-induced electron transfer on lanthanide-based coordination polymers luminescence : A comparison between two pseudo-isoreticular molecular networks. *Inorg. Chem.* **2014,** *53*, 1217-1228.
18. Xu, H.; Dong, Y.; Wu, Y.; Ren, W.; Zhao, T.; Wang, S., An -OH group functionalized MOF for ratiometric Fe^{3+} sensing. *J. Solid State Chem.* **2018,** *258*, 441-446.
19. Desreux, J. F., In *Lanthanide Probes in Life, Chemical and Earth Sciences*, Choppin, G. R.; Bünzli, J. C. G., Eds. Elsevier: Amsterdam, **1989**; Vol. Elsevier, p 43.
20. Henisch, H. K., *Crystals in Gels and Liesegang Rings*. Cambridge University Press: Cambridge, **1988**.

21. Henisch, H. K.; Rustum, R., *Crystal Growth in Gels*. The Pennsylvania State University Press: **1970**, p 1-196.
22. Daiguebonne, C.; Deluzet, A.; Camara, M.; Boubekeur, K.; Audebrand, N.; Gérault, Y.; Baux, C.; Guillou, O., Lanthanide-based molecular materials : gel medium induced polymorphism. *Cryst. Growth Des.* **2003,** *3*, 1015-1020.
23. Abdallah, A.; Freslon, S.; Fan, X.; Rojo, A.; Daiguebonne, C.; Suffren, Y.; Bernot, K.; Calvez, G.; Roisnel, T.; Guillou, O., Lanthanide based coordination polymers with 1,4 carboxyphenylboronic ligand: multi emissive compounds for multi sensitive luminescent thermometric probes. *Inorg. Chem.* **2019,** *58*, 462-475.
24. Luo, Y.; Calvez, G.; Freslon, S.; Daiguebonne, C.; Roisnel, T.; Guillou, O., A new family of lanthanide containing molecular open frameworks with high porosity : [Ln(abdc)(Habdc),2H_2O] with Ln = La -Eu and 8<n<11. *Inorg. Chim. Acta* **2011,** *368*, 170-178.
25. Chen, X. Y.; Zhao, B.; Shi, W.; Xia, J.; Cheng, P.; Liao, D. Z.; Yan, S. P.; Jiang, Z. H., Microporous metal-organic frameworks built on a Ln3 cluster as a six connecting node. *Chem. Mater.* **2005,** *17*, 2866-2874.
26. Weissman, S. I., Intramolecular energy transfer - The fluorescence of complexes of europium. *J. Chem Phys* **1942,** *10*, 214-217.
27. Galaup, C.; Couchet, J.-M.; Bedel, S.; Tisnès, P.; Picard, C., Direct access to terpyridine-containing polyazamacrocycles as photosensitizing ligands for Eu(III) luminescence in aqueous media. *J. Org. Chem.* **2005,** *70*, 2274-2284.
28. Haitao, X.; Nengwu, Z.; Xianglin, J.; Ruyi, Y.; Yonggang, W.; Enyi, Y.; Zhengquan, L., Assembly of lanthanide coordination polymers with one dimensional channels. *J. Mol. Struc.* **2003,** *655*, 339-342.
29. Petrosyants, S.; Dobrokhotova, Z. V.; Ilyukhin, A.; Gavrikov, A.; Efimov, N.; Novotortsev, V., Coordination polymers of rare-earth elements with 2-aminoterephthalic acid. *Russ. J. Coord. Chem.* **2017,** *43*, 770-779.
30. Xu, H. T.; Zheng, N. W.; Jin, X. L.; Yang, R. Y.; Li, Z. Q., Channel structure of diaquasesqui(2-aminoterephthalato)dysprosium(III) dihydrate. *J. Mol. Struc.* **2003,** *646*, 197-199.
31. Xu, H. T.; Zheng, N. W.; Jin, X. L.; Yang, R. Y.; Li, Z. Q., A new microporous structure constructed by a lanthanide-carboxylate coordination polymer. *J. Mol. Struc.* **2003,** *654*, 183-186.
32. Bünzli, J. C. G.; Eliseeva, S. V., Basics of lanthanide photophysics. In *Lanthanide Luminescence*, Hänninen, P.; Härmä, H., Eds. Springer Berlin Heidelberg: **2010**; Vol. 7, p 1-45.
33. Luo, Y.; Zheng, Y.; Calvez, G.; Freslon, S.; Bernot, K.; Daiguebonne, C.; Roisnel, T.; Guillou, O., Synthesis, crystal structure and luminescent properties of new lanthanide-containing coordination polymers Involving 4,4'-oxy-bis-benzoate as Ligand. *Cryst. Eng. Comm.* **2013,** *15*, 706-720.
34. Badiane, I.; Freslon, S.; Suffren, Y.; Daiguebonne, C.; Calvez, G.; Bernot, K.; Camara, M.; Guillou, O., High britness and easy color modulation in lanthanide-based coordination polymers with 5-methoxyisophthalate as ligand: Toward emission colors additive strategy. *Cryst. Growth Des.* **2017,** *17*, 1224-1234.
35. Piguet, C.; Bünzli, J. C. G.; Bernardinelli, G.; Hopfgatner, G.; Williams, A. F., Self-assembly and photophysical properties of lanthanide dinuclear triple-helical complexes. *J. Am. Chem. Soc.* **1993,** *115*, 8197-8206.

TABLE OF CONTENT